Decay Studies of N≃Z Nuclei

Ernst Roeckl

Gesellschaft für Schwerionenforschung, Planckstr. 1, 64291 Darmstadt, Germany, and Institute of Experimental Physics, University of Warsaw, ul. Hoża, 00–681 Warsaw, Poland

Abstract. The decay properties of N≃Z nuclei are reviewed, and their relation to nuclear–structure, astrophysics and fundamental physics is described. Focussing on direct charged–particle radioactivity and β decay, particular emphasis is put on direct proton, two–proton and α emission, superallowed 0^+ to 0^+ β transitions, the Gamow–Teller resonance occurring in β decays near ^{100}Sn, β-delayed proton emission of ^{57}Zn, γ-delayed proton emission of ^{58}Cu, and isomer spectroscopy of ^{74}Kr and ^{94}Ag.

1 Introduction

Nuclei with equal or almost equal number of neutrons and protons are of particular, multidisciplinary interest. As sketched in Fig. 1, the disciplines involved are (i) nuclear–structure physics, in particular effects related to the vicinity of the proton drip–line and to the occupation of identical orbits by neutrons and protons, (ii) fundamental physics, e.g. tests of the standard model of weak interaction by precision measurements of super-allowed 0^+ to 0^+ β–decays, and (iii) astrophysics, concerning e.g. the electron capture

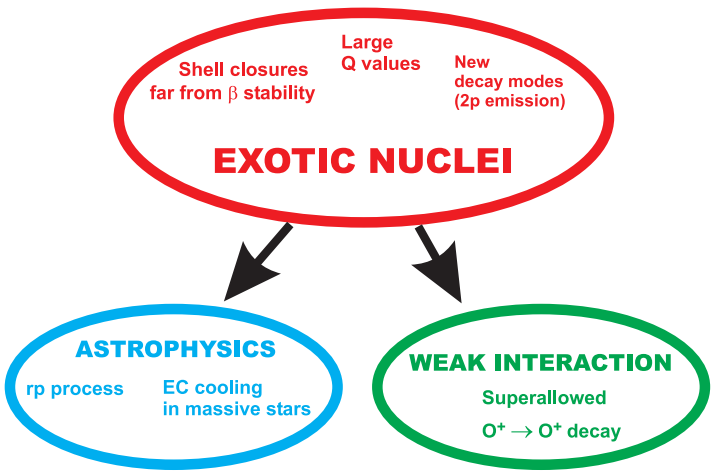

Fig. 1. Links from nuclear–structure features of N≃Z nuclei to the research fields of astrophysics and fundamental physics

E. Roeckl, Decay Studies of N≃Z Nuclei, Lect. Notes Phys. **651**, 223–261 (2004)
http://www.springerlink.com/

(EC) cooling of supernovae or the astrophysical *rp*–process. The experimental progress in these fields has leaned heavily on the use of 'exotic' beams of radioactive ions, and it is thus indeed appropriate to include a discussion of decay properties of N≃Z nuclei into this LNP volume.

The main focus of this report concerns the topic (i) and, in particular, decay properties of nuclei between the double shell closures at ^{56}Ni and ^{100}Sn, some links to the topics (ii) and (iii) being briefly mentioned as well. The special features characterizing nuclei near ^{100}Sn include direct proton and alpha radioactivity,the resonance–like distribution of the Gamow–Teller (GT) β strength, which lies within the decay Q–value, and high-spin isomers. Here and throughout the entire lecture the term 'decay' means a restriction of the lower limit of the lifetime of the initial nuclear state, which is chosen, in an admittedly somewhat arbitrary manner, to generally be longer than 20 ns.

One of the most fascinating aspect in studying N≃Z nuclei (N and Z are the neutron and proton numbers, respectively,) is the search for effects related to neutron–proton pairing. However, as the corresponding measurements hardly involve decay properties, this topic is not included in this report, except for a brief reference to the Wigner term in Sect. 5.

This lecture does not attempt to come anywhere near an extensive and up-to-date review but rather tries to describe the main nuclear–physics phenomena by selecting a few (text–book) examples. A detailed discussion of the nuclear–physics aspects of these results as well as of their relevance to fundamental physics and astrophysics, can not be given within the scope of this report but can be found in the references cited throughout the text. In this context, cross–links to other lectures included in this book are of particular relevance, namely those on the nuclear shell model [1], in-flight separation [2], storage–ring experiments [3], traps for ions and neutral atoms [4], nuclear moments, γ–ray and conversion–electron spectroscopy [5], fundamental interactions [6] and astrophysics [7]. The corresponding refs. [1] to [7] lead the way into the bibliography of this lecture, are thus easily identifiable and can be found by leafing through this book.

The lecture is structured as follows: After a presentation of the experimental observables and the related techniques in Sects. 2 and 3, respectively, Sects. 4 to 9 will contain a discussion of decay properties of ground–states and long-lived isomers of N≃Z nuclei, including direct charged–particle decay, β decay as well as β- and γ-delayed charged–particle emission. Finally, a summary and an outlook will be given in Sect. 10.

2 Experimental Observables and Their Links to Nuclear–Structure Phenomena

2.1 Introductory Remarks on Decay Modes of N≃Z Nuclei

The stability of nuclei requires N=Z for light nuclei whereas beyond N=Z=20 (^{40}Ca) stable nuclei accommodate more neutrons than protons in order to

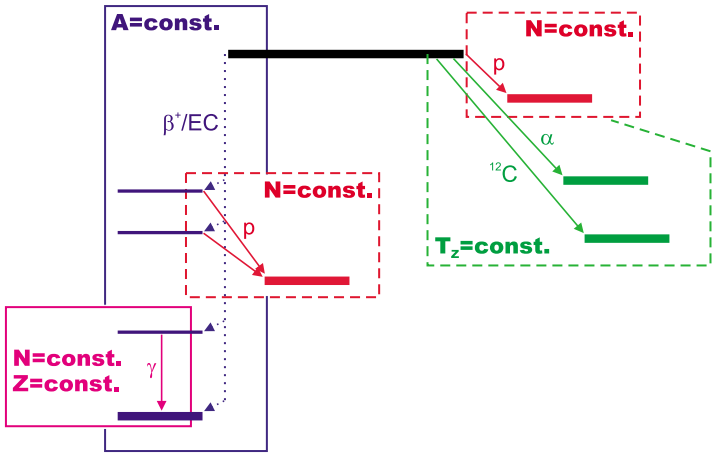

Fig. 2. Decay modes of proton–rich nuclei

outbalance the repulsion of the charged protons. For a minor deviation from the N and Z configuration of neighbouring stable nuclei, β decay occurs, i.e. an excess neutron is transformed into a proton and vice versa. If the imbalance between N and Z becomes too large, the nuclear forces can no longer bind all nucleons and the atomic nucleus becomes unstable against direct charged-particle emission.

The decay modes of N≃Z nuclei are sketched in Fig. 2. One of the basic parameters characterizing nuclear ground states as well as excited levels is their binding energy ('mass'). Under the condition that the atomic mass of a decaying state is larger that that of the daughter state populated in a decay, the or mass difference or Q value of the corresponding disintegration mode is positive, i.e. this decay is energetically possible. Further properties of nuclear states include the radius and other moments, spin and parity (I^{π}), isospin (T) and isospin projection (T_z). As sketched in Fig. 2, direct charged–particle radioactivity involving the emission of protons, α particles or ^{12}C nuclei generally is an isospin–allowed process and so is allowed β decay, whereas the situation is more complicated in the case of β–delayed γ–ray and charged–particle emission (see Sects. 2.3 and 7.3).

The detailed decay properties are routinely updated in the Journal *Nuclear Data Sheets* as well as in other data bases such as Nubase. The latter one has recently been updated [8] together with the evaluation [9] and tabulation [10] of atomic masses which include separation energies and Q values (see also the routine updates issued by the Atomic Mass Data Center [11]).

2.2 Direct Charged–Particle Radioactivity

Basic Features of Direct Charged–Particle Radioactivity. The abovementioned term 'borderline' is related to the separation energy for protons

(S_p), two protons (S_{2p}), α particles (S_α) and other clusters, the related Q values (Q_p, Q_{2p}, Q_α etc.) differing from the respective binding energy only in sign. The chart of nuclides is thus characterized by a multitude of such borderlines, with the emission of protons, two protons etc. becoming energetically possible from the *ground state* of nuclei that are situated beyond the respective borderline (These borderlines can, of course, also be crossed by exciting a given nucleus). The 'direct' (prompt, spontaneous, Coulomb delayed, self-delayed) charged–particle emission from a ground–state or long-lived isomer has to be distinguished from the 'delayed' process in which the prompt emission is *preceded* by a weak interaction ('β-delayed' process) or an electromagnetic transition ('γ-delayed' process[1]).

In the case of direct radioactivity, the emitting nuclear state is *narrow*, i.e. represents a *long-lived* ground state or isomer, whereas in case of the delayed process the emission of charged particles occurs from comparatively *broad*, excited states, the time scale being generally dominated by the initial β decay or at least strongly influenced by the initial γ–ray emission. The excited states referred to here are either in the β–decay daughter(s) or, in the case of γ-delayed charged–particle emission, in the nucleus that is originally produced in the experiment. In both cases the competition with γ de–excitation has to be considered.

At this point, a little digression into semantics may be appropriate. The term 'radioactivity' relates to a time scale which, in the early days of nuclear physics and chemistry, was defined with reference to the time needed for a (chemical) separation. Even nowadays, when the experimentalist claims that a new nuclide 'was shown to exist' he or she generally means that the nuclear species was proven to be long-lived enough to survive the respective separation procedure, and that thus an upper limit for the lifetime of the nucleus of interest can be given. The separation times are generally of the order of microseconds or longer, this lower lifetime–limit for the nuclear state under consideration corresponding to an upper limit of 5×10^{-10} eV for its width. Radioactivity, including that of isomers, is defined in this lecture, with reference to an early review article of Cerny and Hardy [12], as a process characterized by a lifetime larger than 10^{-12} s and hence by a width smaller than 7×10^{-4} eV. This definition is thus linked to the lowest lifetime that can be reached in experiments. The present lecture mainly focusses on properties of such comparatively narrow states (As was mentioned in Sect. 1, this lecture deals with the decay of nuclei whose lifetime are longer than about 20 ns). However, one should keep in mind that a wealth of interesting physics can be and has been learnt by studying *wide resonances* whose widths are larger than the above-mentioned limit of 7×10^{-4} eV and whose lifetimes can thus not be directly measured.

[1] The expression 'γ-delayed charged–particle emission' does not represent a generally accepted term but, to the knowledge of the author, is introduced here for the first time.

Examples of particularly interesting resonance–states are ^{6}Be [13] and ^{8}Be, which are unbound in their ground states, the half–lives and widths amounting to $5.0(0.3)\times10^{-21}$ s, 92(6) keV and $6.7(1.7)\times10^{-17}$ s, 6.8(1.7) keV, respectively [8]. They represent prime cases to study direct two-proton and two-α emission, respectively. Properties of the ^{8}Be ground–state and of the excited 10.7 MeV level in ^{12}C are relevant to the astrophysical interesting triple–α reaction. This ^{12}C state has recently been studied by performing experiments on β^- decay of ^{12}N and β^+ decay of ^{12}B [14]. A corresponding case is ^{9}Be, investigated by ^{9}C [15–17] and ^{9}Li decay [18].

The following discussion of charged–particle decay spectroscopy will start out by describing the direct α decay. It is historically the first charged–particle decay mode discovered, still actively pursued today as impressively proven by the research on isotopes of the heaviest element, and well suited to serve as a basis for the theoretical interpretation of the experimental data on charged–particle radioactivities (see Sect. 2.2): The definitions of barrier transmission probability, reduced width etc., introduced for the direct α decay in Sect. 2.2, will indeed form the basis for interpreting the other charged-particle disintegration modes. Alpha–decay data of nuclei near ^{100}Sn will be presented in Sect. 6.1, followed by a discussion of direct proton (Sect. 6.2) and two–proton (Sect. 6.3) decay.

Direct α Emission: The Model Case for Interpreting Charged–Particle Decay Data. In direct α decay, the experimental observables are

- the α–particle energy which, corrected for the recoil effect, yields the total decay energy (Q_α), i.e a mass link between the parent and daughter state,
- the total half–life ($T_{1/2}$) and
- the α–decay branching ratio (b_α).

From these quantities one deduces the experimental α–decay constant $\lambda_\alpha^{(exp)}$, defined according to

$$\lambda_\alpha^{(exp)} = \frac{b_\alpha \cdot ln2}{T_{1/2}}, \tag{1}$$

which is used for a comparison with the corresponding theoretical quantity $\lambda_\alpha^{(theor)}$. The latter can be determined by means of the semi-classical Gamow approach [19] to be

$$\lambda_\alpha^{(theor)} = \frac{v_\alpha}{R_i} P_\alpha. \tag{2}$$

Here v_α is the velocity of the α particle inside the nucleus, deduced as

$$v_\alpha = \sqrt{\frac{U_0 + Q_\alpha + \Delta E_{scr}}{M_\alpha}}, \tag{3}$$

and P_α the barrier transmission for α particles,

$$P_\alpha = exp\{-2\int_{R_i}^{R_a}\sqrt{\frac{2M_\alpha(U(R)+Q_\alpha+\Delta E_{scr})}{\hbar}}dR\}. \quad (4)$$

The Gamow approach is based on a one-dimensional potential [19,20] of depth U_0 and (Coulomb) barrier shape $U(R)$, with R being the radial dimension. ΔE_{scr} is the screening correction, M_α the mass of the α particle, and R_i and R_a the inner and outer turning points. Equation (4) holds for the s-wave emission of α particles, such as that occurring in transitions from 0^+ to 0^+ states. If the α emission involves non–zero orbital angular momenta (ℓ), an additional ℓ-dependent centrifugal barrier has to be taken into account in (4), which describes the tunnelling through that barrier. Thus P_α and $\lambda_\alpha^{(theor)}$ *strongly* depend on Q_α, as can be easily deduced from (2) to (4), and also on ℓ. This sensitivity arises from the linear dependence of $U(r)$ on the charge of the emitted particle and from the inverse dependence of the centrifugal barrier on M_α. In contrast to α decay, one-proton radioactivity is hence characterized by a relatively low Coulomb barrier and a relatively high centrifugal barrier. A graphical presentation of these barriers for the case of ^{167}Ir can be seen from Fig. 3 of [21]. These feature will again be referred to when discussing one–proton radioactivity further in this section and in Sect. 6.2.

Another valuable information is contained in the spectroscopic factor S_α^{exp},

$$S_\alpha^{exp} = \frac{\lambda_\alpha^{(exp)}}{\lambda_\alpha^{(theor)}}. \quad (5)$$

Within the Gamow model, S_α^{exp} is found to be $4{\cdot}10^{-4}$ [20] for the decay of ^{212}Po to the ground state of its doubly magic daughter, ^{208}Pb. The latter transition is generally used as a reference for comparing α–decay data. This low S_α^{exp} value is indicative of the small probability of the formation of an α particle inside a nucleus. It will be interesting to inspect the corresponding quantity for the case of direct proton and two-proton decay (see Sects. 6.2 and 6.3).

Furthermore, the reduced width W_α, defined as

$$W_\alpha^{exp} = \frac{\lambda_\alpha^{(exp)}}{P}, \quad (6)$$

can be used as a basis for systematically comparing α–decay data. The W_α systematics of even-even (0^+) nuclei, normalized to the above-mentioned decay ^{212}Po, may serve as an example. It shows that the *large range* of experimental Q_α, $T_{1/2}$ and b_α data is reduced to a rather *smooth variation* of W_α, i.e. a regular staggering with respect to the Z=50, N=50 and Z=82, N=126 shell–closures: The W_α values for 0^+ to 0^+ α–decay actually vary by a factor

of only about 60 (see Fig. 5.1 of [20]), which signals a remarkable success of the semi-classical Gamow model.

A particularly interesting phenomenon of α decay is the occurrence of fine structure, i.e. α transitions to excited states in the daughter nucleus. The corresponding data are interpreted by using a hindrance factor which is deduced as the ratio between the W_α values found for the transitions to the ground state and excited state.

As an aside, it is interesting to note that the upper end of the range of α–decay half-lives has recently been set by de Marcillac et al. [22]. They succeeded to detect α emission of ^{209}Bi, an isotope considered hitherto to be stable. The half-life was found to be $1.9(0.2)\times10^{19}$ y, which is about a factor of 10^9 longer than the age of the universe. The experiment confirmed the previously known [10] Q_α value of 3137.2(0.8) keV. The nucleus ^{209}Bi, a single–proton configuration with reference to the doubly closed–shell core ^{208}Pb, has a comparatively small Q_α value as its α decay proceeds 'across' the Z=82 shell–closure. The underlying cusp–like structure of the mass–energy surface near ^{208}Pb will serve as a reference when discussing Q_α values near the double shell closure at ^{100}Sn (see Sect. 6.1). While the latter nucleus is bound with respect to α emission, the former has a small, but positive Q_α value of 516.9(1.3) keV [10]. The corresponding α–decay half-life is so much beyond the age of the universe that it will certainly be outside the range of experiments for quite some while and that, for the time being, ^{208}Pb can thus be safely called a 'stable isotope'.

Direct Proton and Two–Proton Emission. The possibility of one–proton and two–proton radioactivity has first been discussed by Goldanskii in 1960 [23]. The idea has been that a sufficiently large proton excess would lead to one–proton radioactivity of odd-Z and two–proton radioactivity of odd-Z nuclei, this selectivity being related to both the pairing effect on the mass energy surface and the strong energy dependence of the tunneling process (see Sect. 2.2).

Direct one–proton emission was first observed in 1970 as a weak (1.5 %) decay branch of a long-lived (245 ms) isomer of ^{53}Co [24] and, in 1981, as emission from the ground states of ^{147}Tm and ^{151}Lu. The latter experiments were performed at the Separator for Heavy–ion Products [25] and the ISOL facility [26] of GSI Darmstadt. It has become clear already from these early experiments that the data on direct proton emission, i.e. Q value, half–life and branching ratio, can be conveniently interpreted on the basis of the Gamow theory introduced in Sect. 2.2, i.e. by deducing quantities such as spectroscopic factor, reduced width or hindrance factor in analogy to the corresponding α–decay parameters. As was mentioned above, the Gamow approach is based on a nuclear potential of spherical symmetry. Thus, the spectroscopic factors of the order unity that are found in this way, e.g., for the ground–state decays of ^{147}Tm and ^{151}Lu indicate transitions of a readily 'preformed'

proton in a near-spherical $\pi h_{11/2}$ shell–model state. The strong l dependence of the one-proton decay constant, calculated in analogy to (1) to (4), was already mentioned above. As an example, the theoretical half–life of ^{147}Tm, deduced in analogy to (1) for a proton energy of 1051 keV, is 28 ms for l=0 and 470 s for l=5 [26].

Two–proton emission is conceptually different from one–proton radioactivity as ^{2}He is unbound. If the one–proton daughter state lies lower in energy than the emitting state, a *sequential* emission of the two protons occurs, provided it can proceed through a well-defined intermediate state. Several cases of this type of disintegration mode have already been observed (see, e.g., [27, 28]). If condition concerning the intermediate state is not fulfilled and, in particular, if one–proton emission is energetically forbidden, the two protons are emitted *simultaneously*. In this case, commonly referred to as *two–proton radioactivity* (see also the remarks on semantics above), the experiment has to clarify whether there is a strong correlation in energy and angle between the two protons, which would identify a process usually called '^{2}He emission', or whether they are emitted independently with the only restriction being phase space, referred to as 'three–body decay' (see Sect. 6.2).

Similar to other charged–particle decay modes, a strong dependence of the half–life for two–proton radioactivity upon the Q_{2p} value is expected. For the case of ^{45}Fe, for example, it is predicted on the basis of a Gamow–like model, assuming tunnelling of two–protons and a spectroscopic factor of unity, that Q_{2p} values of 1.0 and 1.3 MeV correspond to half–lives of 10^{-3} and 4×10^{-7} s, respectively [29] (see Sect. 6.2).

2.3 Beta Decay

Basic Features of β^+/EC Decay. While a more extended discussion of weak interaction is given in [6], some of the main features of β^+/EC decay will be briefly described here. The competition between positron emission an EC is governed by a 2nd and 5th power dependence on the decay energy, respectively. Thus the latter quantity can be determined by measuring the ratio of β^+ and EC transitions (see Sect. 3.4). Electron–capture transitions can be experimentally identified by detecting characteristic X–rays of the decay daughter, provided they are distinguished from X–rays originating from conversion of β-delayed transitions.

Above the threshold for proton emission, the latter process competes with γ–ray emission from excited levels. Thus, β–delayed γ–rays occur either in the daughter nucleus or from states in nuclei populated by charged–particle emission (see Fig. 3). The information gained from such electromagnetic de–excitations complements that obtained by means of in–beam spectroscopy, the latter method generally being restricted to high–spin states (see [5] and Sects. 8 and 9.2).

Ever since its discovery in 1969 [30], β-delayed emission of charged particles has continued to be a valuable research tool, delivering rich nuclear–

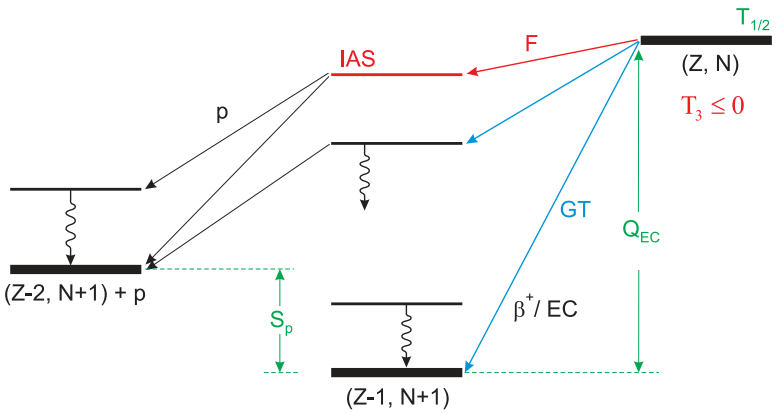

Fig. 3. Sketch of the basic decay scheme for allowed and superallowed β decay, including the emission of β-delayed γ–rays and protons

structure data. The properties investigated concern levels in the original, intermediate and final nucleus as well as, e.g., their (binding) energy, spin, parity and lifetime. In this way, complementary information can be gained to that obtained by studying β–delayed γ–ray emission or performing in-beam or reaction spectroscopy (see [31–33] for recent reviews). Insight into the lifetime (and ratio between radiative and proton widths) of the proton-emitting levels can be gained by means of the proton X–ray coincidence technique [34].

Beta-delayed particle spectra are characterized by distinct lines for light nuclei (see, e.g., the cases of ^{33}Ar mentioned below or of ^{57}Zn discussed in Sect. 7.3), but are of more or less continuous bell–shape for heavy nuclei such as ^{94}Ag (see Sect. 9.2). A particularly interesting aspect, even though not discussed in this lecture, is the test of isospin symmetry for well bound states versus those of resonances (see, e.g. the work on the A=9 [15–18] and A=12 systems [14]).

Nuclear β decay is conveniently characterized by using the ft value which is inversely proportional to the 'strength' B that in turn is defined as the square of the relevant β–decay matrix element,

$$ft \propto \frac{1}{B}. \tag{7}$$

The statistical rate function f depends strongly on the Q value for β decay but not in other nuclear-structure properties, and t is the partial half-life, determined by the total half-life of the nucleus under consideration as well as its β–decay branch.

As far as allowed β decay is concerned (see Fig. 3), one distinguished between super-allowed (Fermi) transitions and ordinary allowed GT transitions, the corresponding strength being B_F and B_{GT}. The isospin formalism allows

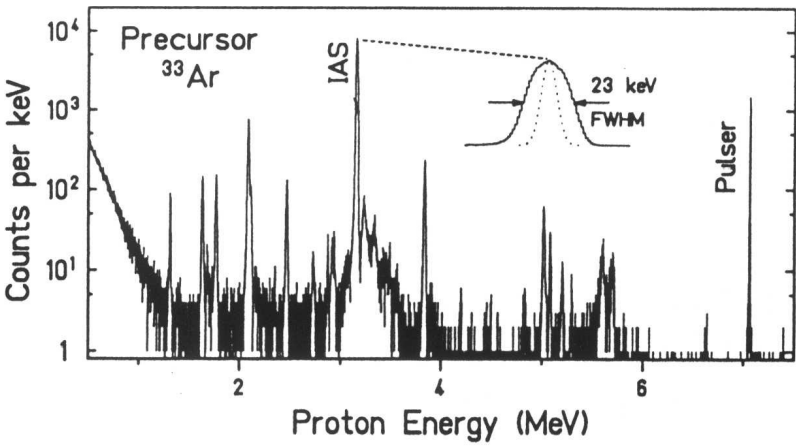

Fig. 4. Energy spectrum of β–delayed protons measured for the decay of ^{33}Ar. The dominant 3.167 MeV line is due to proton emission from the IAS in ^{33}Cl to the 0^+ ground–state of ^{32}S, while most of the other lines are related to GT decay. The inset shows that for this line the recoil broadening of 23 keV FWHM is considerably larger than the detector resolution of 8 keV FWHM [35]

one to assign an isospin T, which is part of an isobaric multiplet (see also Sect. 5). All members of a multiplet have identical wave functions, provided isospin symmetry is conserved. Fermi β decay is governed by the isospin–flip operator (τ_+, τ_-), with β^+/EC decay involving the (σ_-) operator. The selection rules of Fermi transitions are ΔI=0, $\Delta\pi$=0, ΔT=0, and ΔT_z=1. Thus they connect isobaric analog states. A particular such state, abbreviated IAS, is the daughter state of a Fermi β decay (see Fig. 3). For parent nuclei with $T_z \leq 0$, excluding even-even ones with N=Z, the IAS lies within the Q_{EC} window, forming the ground state in case of the 0^+ to 0^+ decay of N=Z, odd-odd nuclei (T=0, T_z=1), see Fig. 3.

Gamow-Teller transitions are governed by the spin-flip (σ) and isospin–flip operators, with the selection rules being ΔI=0 or 1 (I=0$\rightarrow$I=0 excluded), $\Delta\pi$=no, ΔT=0, and ΔT_z=1. While Fermi transitions are characterized by antiparallel spins of positron and antineutrino, and by the tendency of the two leptons of being emitted collinearly, the opposite holds for GT decay.

A text-book example for the distinction between Fermi and GT transitions is the measurement of the decay of ^{33}Ar (T_z=$-3/2$), performed by Schardt and Riisager [35] at the ISOLDE Facility of CERN, Geneva. The β-delayed proton spectrum of ^{33}Ar, obtained in this work, is displayed in Fig. 4. Due to the different angular correlations between positron and antineutrino in the two disintegration modes, the Doppler effect introduces a larger recoil broadening of the proton lines for Fermi than for GT decay (Such Doppler effects occur, of course, only under the condition that the proton is emitted *before* the recoil nucleus ^{33}Cl comes to rest). It is indeed

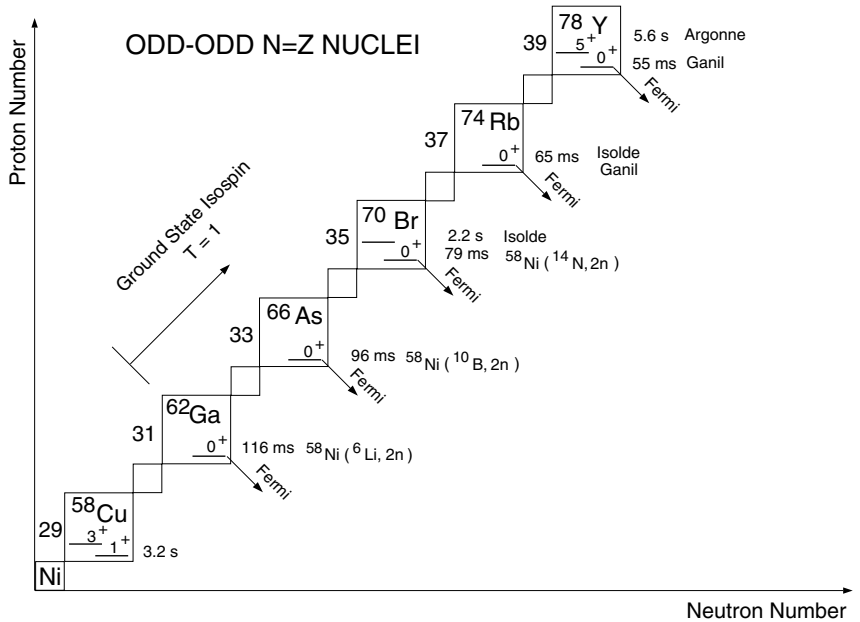

Fig. 5. Compilation of decay properties of odd-odd N=Z nuclei from A=58 to A=78. The experimental half-lives, production reactions and relevant laboratories are indicated, based on the status of this research in 2000 (see [38] for detailed references to the experimental works involved)

impressive to see the strikingly larger width of the proton line stemming from the IAS, compared to the line widths related to GT decay. An even more impressive, recent example is the broadening of the proton line following of the 0^+ to 0^+ β–decay of ^{32}Ar (see Fig. 4 of [6], taken from [36,37]). Thus the β-delayed protons can be used as a 'magnifying glass' for observing such recoil effects in a *singles* spectrum, i.e. without the need for using polarized atoms and/or a directional-coincidence measurement. Meanwhile, the pioneering work of Schardt and Riisager has already been followed up by dedicated experiments [36,37] which aim at searching for scalar contribution to the weak force (see also [6]).

We note in passing that the emission of protons (T=1/2, T_z=1/2) from the IAS in ^{33}Cl (T=3/2, T_z=−1/2) to the (low-lying) states of lowest isospin in the proton-daughter ^{32}S (T=0, T_z=0) are isospin-forbidden, whereas the β-delayed proton emission following GT decay is isospin-allowed. This holds also for the decay of ^{57}Zn which belongs to the same T=3/2, T_z=−3/2 series as ^{33}Ar and will be further discussed in Sect. 7.3.

In Fig. 5, the decay modes of odd-odd N=Z nuclei from A=58 to A=78 are sketched. While ^{58}Cu has a deuteron-like $I^\pi=1^+$,T=0 ground-state, ^{62}Ga and heavier nuclei of this series posses a $I^\pi=0^+$,T=1 ground-state. Long-lived

isomers occur in ^{58}Cu, ^{70}Br, ^{78}Y and, as will be discussed in Sect. 9, also in ^{94}Ag. Except for the case of ^{58}Cu they all disintegrate predominantly by β^+/EC decay rather than by internal transitions.

Fermi β Decay. The cases of Fermi β decay, that are discussed in this report to some detail, concern ^{57}Zn (T=3/2, T_z=−3/2), see Sect. 7.3, as well as the series of 0^+ to 0^+ decays of T=0, T_z=1 nuclei, see Sect. 7.1. As will be discussed in the latter section, the Fermi coupling constant G_F is most precisely determined from the decay of nine isotopes ranging from ^{10}C to ^{54}Co [39,40]. The 0^+ to 0^+ Fermi decays of these isotopes allow one to determine a corrected Ft value from the ft values of the individual isotopes and thus the coupling constant G_F by means of the relation [39]

$$\mathcal{F}t = ft(1+\delta_R^{'})(1+\delta_{NS}-\delta_C) = \frac{k}{2G_F(1+\Delta_R^V)}. \tag{8}$$

The quantities $\delta_R^{'}$, δ_{NS} and δ_C are the nucleus dependent part of the radiative correction, the nuclear structure dependent radiative correction, and the isospin–symmetry breaking correction, respectively, k is a constant $(k/(\hbar c)^6 = (8120.271\pm0.012)\times10^{-10} GeV^{-4}s)$ and Δ_R^V is the transition independent part of the radiative corrections. Equation (8) is based on a B_F value of 2.

The corrected $\mathcal{F}t$ values allow one to test the conserved vector–current (CVC) hypothesis of the weak interaction and to study the unitarity of the Cabbibo–Kobayashi–Maskawa (CKM) quark mixing matrix. This topic will be further discussed in Sect. 7.1.

Gamow-Teller β Decay. For a pure GT decay the strength can be calculated according to

$$B_{GT} = \frac{D}{ft}, \tag{9}$$

with D=3860(18) s denoting a parameter corresponding to the axial–vector coupling constant which is deduced from the β decay of the free neutron [41–43]. Nuclear-structure features of the mother and daughter nucleus of interest are studied by comparing the experimental B_{GT} values with the corresponding model predictions. In this comparison, one has to take the Q–value limitation of the experimental data into account. The theoretical limitations are based, e.g., on the shell model (see [1,44] and the discussion below).

In the β decay of heavy nuclei, there are often many (close-lying) levels in the daughter nucleus populated, resulting in a correspondingly broad and continuous β–strength distribution. In this case, it is generally appropriate to use *average* B_{GT} values which refer to a certain interval of the excitation energy of the daughter nucleus and are thus given in inverse energy units. The experimental observables are then the distribution of such average B_{GT}

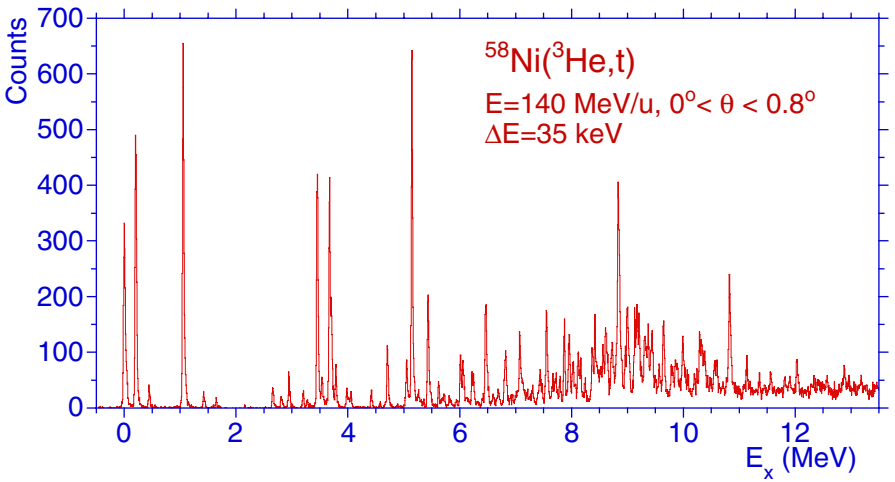

Fig. 6. High-resolution spectrum obtained by using a 140 MeV/u ^{3}He beam to study the ^{58}Ni(^{3}He,^{3}H) reaction. The energy resolution for detecting ^{3}H ejectiles amounted to 35 keV FWHM. The abscissa represents the excitation energies in ^{58}Cu, derived from the experimental ^{3}H energies. The ^{3}H ejectiles were measured within an angular acceptance of $\pm 0.4^{0}$ with respect to the direction of the ^{3}He beam [46]

values as a function of the excitation energy in the daughter nucleus as well as the total B_{GT} strength (ΣB_{GT}), integrated over the total Q value or the experimentally covered range of excitation energies. Correspondingly, the 'averaged' B_{GT} and the ΣB_{GT} values are compared with theory.

This may be the proper context to remind the reader of the 'Pandemonium' problem. Pandemonium stands for a fictitious nucleus which has been introduced by Hardy et al. [45] in order to demonstrate the difficulty of performing *complete* high–resolution spectroscopy in the case of the β decay of heavy nuclei which generally involves a large number of closely spaced levels in the respective daughter nuclei. This topic lead to heated discussions in the late seventies and early eighties, which evidently have cooled off meanwhile, even though the problem concerning the reliability of the determination of 'apparent' β intensities from experimental data definitely needs continuing attention.

Concerning the GT β–decay measurements discussed in this lecture, the recent ^{58}Ni(^{3}He,^{3}H) data [46], displayed in Fig. 6, may serve to illustrate the question of high-lying versus low-lying GT strength. The data stem from the an experiment performed by means of the magnetic spectrograph Grand Raiden of the RCNP, Osaka. The peaks observed in this spectrum are generally assigned to GT tansitions, except for that at 0.3 MeV which stems from a Fermi transition. In this type of measurement, the intensity of lines interpreted as GT transitions are assumed to be proportional to the corre-

sponding strenghts, whereas a different scaling law applies for the intensity of the Fermi transition. One the one hand, β–decay data are used to calibrate the GT scaling of such data from charge–exchange reaction. On the other hand, it is evident from Fig. 6 that only the low–energy tail of the GT single-particle resonance can be reached by β–decay experiments on fp–shell nuclei, if they are restricted to Q values of a few MeV.

A particularly interesting feature of nuclei 'southeast' of ^{100}Sn is that their β decay is expected to be characterized by a fast $\pi g_{9/2}$ to $\nu g_{7/2}$ GT transition. Within the extreme single-particle shell model, such transitions involve protons in the mostly filled $g_{9/2}$ orbital, with the corresponding GT partner shell $\nu g_{7/2}$ being mostly empty. This model predicts the ΣB_{GT} value to be

$$\Sigma B_{GT} = \frac{N_{9/2}}{10} \cdot (1 - \frac{N_{7/2}}{8}) \cdot B^0_{GT}, \tag{10}$$

where $N_{9/2}$ denotes the number of protons filling the $g_{9/2}$ orbit, $N_{7/2}$ the corresponding value for the $\nu g_{9/2}$ orbit, and $B^0_{GT} = 17.78$ the ΣB_{GT} value of ^{100}Sn. The latter quantity yields, according to (2), an ft value of 208 s, i.e. a factor of about 15 *smaller* than that of the Fermi 0^+ to 0^+ transitions (see Sect. 2.3). This would mean that the GT β–decay of ^{100}Sn would be considerably *faster* than the superallowed transition. Furthermore, in contrast to the ^{56}Ni region, the GT resonance is expected to lie within the Q–value window for the β decay of nuclei below ^{100}Sn, as will be discussed in Sect. 7.2. What makes the case of ^{100}Sn even more interesting is the prediction [47] that the GT strength is concentrated in essentially one single 1^+ state of ^{100}In 'super GT resonance'. As will be shown in Sect. 7.2, the ΣB_{GT} values measured for nuclei 'southeast' of ^{100}Sn are found to be significantly smaller than those from theoretical predictions. This 'hindrance' or 'quenching' of GT transitions can be expressed as the ratio between the theoretically and experimentally determined GT strength (see Sect. 7.2).

The super GT resonance is a *single–particle* feature that occurs at *low* excitation energy of the daughter nucleus. This phenomenon should not be confused with the *high-lying, collective* GT strength which is investigated by means of charge–exchange reaction. As an example, Fig. 6 displays the GT strength (spin–isospin excitations) in ^{58}Cu, obtained by means of ^{58}Ni(^{3}He,^{3}H) reactions. Compared to β–decay studies, the advantages of using charge–exchange reactions are that they do not suffer from Q–value restrictions and that spin–isospin excitations can be studied both 'in β^+ direction' (by means of (p,n) or (^{3}He,^{3}H) reactions) and 'in β^- direction' (by means of (n,p) or (^{2}H,^{2}He) reactions). The sum of the resulting ΣB_{GT} data can then be compared to the value of 3(N-Z) predicted by the Ikeda sum rule. The disadvantages are that radioactive target nuclei are excluded (so far) and that the task of deducing B_{GT} values from experimental cross–section is not straightforward. The most recent results obtained by using ^{70}Zr(p,n) [48] and ^{70}Zr(n,p) [49] reactions the ΣB_{GT} values in β^+ and β^- direction exhaust approximately 90 % of the Ikeda sum–rule strength.

2.4 Link to Astrophysics

There are many links between the nuclear structure of N≃Z nuclei and astrophysics [7], including the following topics:

- The β^+ decay of ^{12}N allows one to study the 10.7 MeV level in ^{12}C which is the threshold state of the triple–α reaction (Sects. 2.2 and 2.3).
- Concerning EC cooling of supernovae [7,50,51], the GT data deduced from β^+/EC measurements (see Sects. 7.2 and 7.3) are of interest. They do, however, not directly yield relevant strength (but rather that of the isospin–mirrored transitions) but help to improve the (shell–model) calculations used for astrophysical purposes. In this respect, results from β^+/EC experiments compliment those obtained by studying charge–exchange reactions (see, e.g., Sect. 4.1 and Fig. 5 of [7]).
- Calculations of the astrophysical *rp*–process path [7,52] are mainly determined by nuclear masses and β–decay rates of N≃Z nuclei, with α decay beyond ^{100}Sn determining the endpoint of the process. In this context, the data presented in Sects. 4, 5, and 6.1 are relevant. Moreover, the role of isomers is of interest (see Sect. 9.1).

3 Experimental Techniques

The experimental techniques covered in this lecture range from in–beam to in–flight [2], recoil–separation and isotope separation on-line (ISOL) methods. As a sizable fraction of the measurements discussed in this lecture stem from the ISOL facility of GSI Darmstadt (GSI–ISOL), it may be appropriate to have a closer look at this instrument, the development of ion sources and detector arrays being representative for what is pursued at other laboratories.

3.1 The GSI–ISOL Facility

At the GSI–ISOL facility [53], heavy-ion induced fusion–evaporation reactions between ^{32}S, ^{36}Ar, ^{40}Ca or ^{58}Ni beams and ^{28}Si, ^{40}Ca, ^{50,52}Cr or ^{58,60}Ni targets are exploited. Chemically selective ion sources from the FEBIAD [54, 55] or TIS [56] type are used to produce mass-separated beams of neutron-deficient iron–to–barium isotopes as singly-charged atomic or molecular ions [57]. The 55 keV beams are implanted either into a thin carbon foil, 'viewed' by a detector, or into a tape that transports the activity to (or away from) a detector. Detailed spectroscopic studies have been performed down to intensities of a few atoms/min for the mass-separated beams of interest. Examples for measurements based on such low–intensity beam concern, e.g., ^{57}Zn [58], ^{101}Sn^{32}Sn [59,60] and ^{114}Ba^{19}F [60,61], as will be discussed in Sects. 7.3, 7.2, and 6.1, respectively. The latter two examples are particularly interesting: The technique based on molecular–ion formation [57] allows one to strongly suppress isobaric contaminants which opens exciting new possibilities for decay studies of, e.g., light tin and barium isotopes, including maybe even ^{100}Sn.

3.2 Charged–Particle Detection

Direct or β-delayed emission of protons and α particles is generally studied by means of ΔE–E telescopes consisting of a thin gas or silicon (Si) ΔE–detector and a thick Si E–detector. The former records the energy loss of β–delayed charged particles, whereas the latter measures their rest energy. Directly emitted (low–energy) protons or α particles are stopped in the thin detector, with positrons being recorded in the thick detector to derive an anti–coincidence condition and to thus suppress energy–loss events of β-delayed particles. The advantage of silicon detectors is that they combine the attractive feature of good energy resolution, large detection efficiency and high signal–to–background ratio.

As alternatives for recording positrons, plastic–scintillation detectors or Si strip detectors are being used. A particularly interesting recent development of the latter type is a close to 4π array for the simultaneous measurement of positrons and protons [62].

3.3 High–Resolution γ–Ray Detection

The *high–resolution* spectroscopy of β-delayed γ rays emitted from the mass-separated sources is accomplished by using germanium (Ge) detectors, including those of the Euroball–Cluster and Clover type (see [5] for a discussion of γ-ray spectroscopy based on Ge detectors). An exceptionally efficient high–resolution γ–ray detector was available at the GSI–ISOL facility in 1996. It consisted of a cube-like array of 6 Euroball-Cluster detectors (Cluster Cube) which comprised 42 Ge crystals and had an absolute photo–peak efficiency of 10.2(0.5) % for 1.33 MeV γ–rays [63]. In subsequent experiments, β-delayed γ–rays emitted from weak sources were measured by operating similar Ge arrays in coincidence with positrons. The latter radiation was recorded by using detectors such as those mentioned in Sect. 3.2.

The problem of high–resolution Ge detectors is that they may miss a sizeable fraction of the intensity of β-delayed γ rays, e.g those (high–energy) ones from the (quasi-statistical) de–excitation of high-lying states in the daughter nucleus that are weakly populated in β decay (cf. the discussion of the pandemonium problem in Sect. 2.3). This is particularly severe when measuring the decay a heavy nucleus far from stability, which involves low source strengths, large decay Q–values and, correspondingly, a high density and thus a large number of excited levels in the daughter nucleus.

3.4 Total Absorption Spectroscopy

As a *low–resolution* but high–efficiency alternative to the γ–ray detectors described above, a total–absorption spectrometer (TAS) is used at the GSI–ISOL facility. The TAS [64] consists of a large NaI crystal surrounding the radioactive source, two small Si detectors above and below the source, and

one Ge detector placed above the upper Si detector. By demanding coincidence with signals from the Si detectors, the β^+–decay component for the nucleus of interest is selected, whereas a coincidence condition with characteristic $K_{\alpha,\beta}$ X–rays recorded by the Ge detector can be used to select the EC mode. By using the summation of γ–ray cascades in the TAS, the *complete* distribution of the β_+/EC intensity as a function of the excitation energy of the daughter nucleus can be determined, including in particular high-lying levels of the respective daughter nuclei. Thus the problem of missing γ intensity, mentioned in Sect. 3.3, can be solved, making the TAS indeed a 'non–pandemonic' instrument [65].

Another interesting feature of the TAS is that the Q_{EC} value can be deduced from the ratio between β^+ and EC intensities. Moreover, the TAS enables one to investigate X rays related to the emission of conversion electrons (from isomeric transitions), with an optional anti–coincidence condition on signals from the Si detectors and the NaI crystal in order to suppress (room) background. Last not least, the TAS can also be used to measure β-delayed protons, detected in one of the Si detectors (or a telescope of Si detectors) which are operated in coincidence with positrons, X rays and/or γ rays. In this way, one can, e. g., distinguish between β^+ and EC transitions preceding proton emission, determine the (Q_{EC}-S_p) value for a selected level of the final nucleus populated by proton transitions, deduce information on the lifetime (and ratio between radiative and proton widths) and of the proton-emitting levels by means of the proton X–ray coincidence technique (see Sect. 2.3), and use proton–γ coincidence data to identify properties of states in the nucleus populated by the proton emission [66,60,67] (see also Sect. 9.2).

4 Isotope Hunting

The first step in studying an exotic nucleus is generally its identification as being long-lived enough to survive the respective separation procedure (see also Sect. 2.1). This 'isotope hunting' will be briefly discussed here by taking the example of light bromine (Z=35), krypton (Z=36) and rubidium (Z=37) isotopes.

In the late sixties, the pioneering work of the Orsay Group[2] lead to isotope identification by using the chemical selectivity of the ISOL ion source and counting ions of mass–separated beams. Thus, the simple appearance of a peak in the mass spectrum corresponds already to the determination of a half–life limit for the particular nucleus. In this way, long isotopic chains of alkali isotopes have been investigated, including the lightest rubidium isotope

[2] The table–top ISOL instrument of the Orsay Group, moving like a 'travelling circus' from one accelerator to the next, has indeed yielded important contributions to the field of exotic–beam physics in its early days. Beyond the mere identification of new isotopes, the so-called 'orsaytopes' [68], the method was also used to determine other ground–state properties.

known at that time, ^{76}Rb [69]. In the seventies experiments at the ISOL facility ISOLDE at CERN lead to the identification of ^{75}Rb [71] and the N=Z, T=0 nucleus ^{74}Rb [72] (More recent data on ^{74}Rb will be discussed in Sect. 7.1).

In recent years, in–flight facilities have played an increasingly important role in isotope hunting. They yield particle–identification plots which display the events identified in–flight on an energy–loss versus time–of–flight plane. In this way the proton dripline can be delineated. An example for the case of ^{78}Kr fragmentation is shown as Fig. 1 of [73], which is also reproduced as Fig. 2 of [2]. These data, together with systematics of production cross–sections, corroborate the earlier conjecture [74] that ^{69}Br as well as ^{73}Rb have half–lives below 24 and 30 ns and are hence unbound against direct one–proton emission by at least 500 and 680 keV, respectively [73]. Thus, isotope–hunting experiments are able to yield quantitative information on the nuclear mass–energy surface (see also [75–79] for the identification of heavier proton–dripline nuclei).

The finding that ^{69}Br is proton unbound means that the astrophysical rp process has to wait for the decay of the comparatively long-lived (1.6 min) nucleus ^{68}Ge before it can continue to heavier masses (see [73,74,79] for a detailed discussion of this aspect).

5 Determination of Nuclear Masses

Nuclear masses are of importance for almost all of the nuclear–structure, funda-mental–physics and astrophysics aspects discussed in this lecture. Mass measurements involve either 'direct'[3] methods, including those based on storage rings [3] or traps [4], or the determination of mass differences as Q values of decays (see Sect. 7.2) or reactions. In recent years, both storage–ring and trap measurements have indeed been very successful in determining both a large number of new masses of nuclei far from stability and a few key masses of fundamental interest (see Sect. 7)[4].

A recent review of the experimental and theoretical determination of nuclear masses can be found in [80]. In addition to the various theoretical models used to predict nuclear masses, there are the following three phenomena that influence the masses of N≃Z nuclei and are thus suited to predict them

[3] The term 'direct mass measurement' refers to the fact that, in contrast to Q–value measurements, properties of the ion of interest such as energy, time–of–flight or revolution frequency are determined in a 'direct' fashion. However, as mentioned in [80], the distinction between 'direct' and 'indirect' mass measurements is somewhat academic as both of them need a calibration of the mass scale.

[4] In spite of the success of recent mass measurements, it is still true that, as was said in 1995 [70], it is a challenge to nuclear theory to match the accuracy reached by the novel mass–spectrometric techniques: The challenge to theory still seems to continue...

and/or to get insight into nuclear–structure properties in this section of the nuclidic chart:

- Mean–field calculations, including the 'macroscopic' approach of the liquid–drop type, reveal that, even when pairing of like nucleons is taken into account, an additional binding effect of about 2 MeV occurs for nuclei with N=Z. This so-called *Wigner term* is highly localized, being thus similar to the shell–correction term of microscopic-macroscopic models, and dies out rapidly as —N=Z— increases from zero. One would immediately tend to ascribe the Wigner term to neutron–proton pairing. However, it is not clear at present to which extend the T=0 and T=1 pairing modes are responsible (see, e.g., [81]).
- *Coulomb–energy systematics* can be used to determine the mass of a proton–rich nucleus from that of its neutron–rich mirror. For example, Brown et al. [82] performed Hartree–Fock calculations to predict masses of N≃Z nuclei in the range 41≤A≤75, which are partly unbound and of interest for rp–process calculations.
- The energy differences between members of isobaric isospin multiplets (see Sect. 2.2) are very well described by *isobaric–multiplet mass equation* which represents a power expansion to second order in T_z. The corresponding three coefficients of all measured multiplets have been tabulated [83]. The quadratic form has recently been confirmed for A=32 and A=33 by precise measurement of the ground–state masses of ^{32}Ar and ^{32}Ar [84], which are also of interest for β–neutrino correlation experiments (see Sect. 2.3).

6 Experiments on Direct Charged-Particle Emission

It is interesting to note that so far, leaving aside a few exceptions, charged–particle decay spectroscopy on N≃Z nuclei has been the domain of fusion–evaporation reactions, induced by stable–isotope heavy–ion beams, and also the domain of experimental methods involving ISOL or magnetic recoil separation.

6.1 Experiments on Direct α Emission Above ^{100}Sn

The occurrence of an island of direct α emission for nuclei situated above or, with reference to the chart of nuclei, 'north–east' of ^{100}Sn is clearly related to the doubly closed–shell character of this nucleus. Most of the recent data stem [86,61] from the GSI–ISOL facility. They concern almost entirely ground–state to ground–state transitions and thus give some insight into the mass–energy surface near ^{100}Sn: The *increase* of the Q_α values along the chain ^{114}Ba-^{110}Xe-^{106}Te-^{102}Sn (see Fig. 7) resembles the well-known 'kink' of the mass-energy surface in the ^{208}Pb region (see Sect. 2.2), and thus represent a text-book example of an experimental evidence for a double shell-closure far

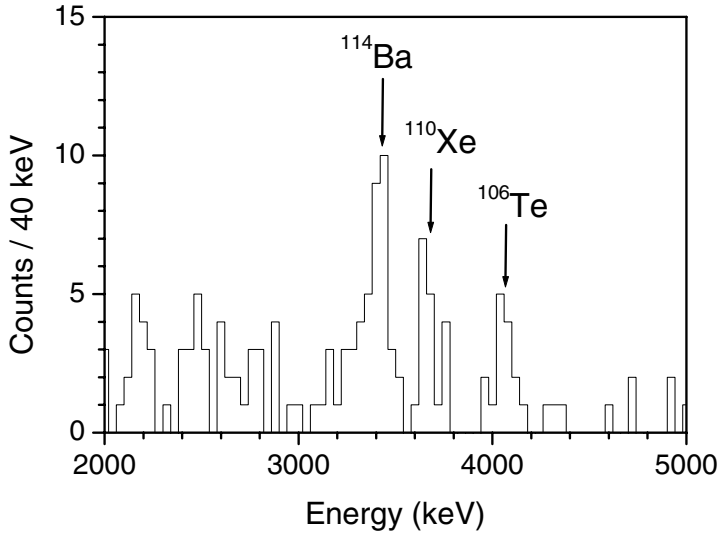

Fig. 7. Energy spectrum of α particles, measured for the decay of ^{114}Ba [61]

from α stability. Moreover, the experimental data displayed in Fig. 7 allow one to deduce an experimental Q value for ^{12}C decay of ^{114}Ba [61]. This result represents an important input–parameter for theoretical estimates of the branching ratio for this cluster disintegration mode which has been firmly established for nuclei above ^{208}Pb but not observed for those above ^{100}Sn so far.

The half–life of ^{106}Te was found to be as low as 60^{+30}_{-10} μs by measuring time–correlated events of consecutive α decays [86]. This shows how small the half–life of a nucleus, whose decay is dominated by direct α emission, becomes for Z=52 and a Q_α value of 4290(9) keV (see the discussion of the Gamow theory in Sect. 2.2). So far, the W_α data for even-even nuclei in this region (^{114}Ba, ^{110}Xe, ^{106}Te) do not yield evidence for the so-called 'super-allowed' α decay. The latter disintegration mode has been suggested in the seventies to occur for nuclei beyond ^{100}Sn in view of their enhanced spatial overlap for protons and neutron that are expected to occupy identical shell–model orbitals.

The interest in fine–structure studies can be exemplified by looking at the case means of ^{107}Te which was investigated by Seweryniak et al. [87] at the Fragment Mass Separator of the Argonne National Laboratory. The resulting α energy spectrum, displayed in Fig. 8, yields evidence for a fine–structure transition with a relative intensity of 0.47(9) %, which populates an excited 168 keV state in the daughter nucleus, ^{103}Sn. This finding is confirmed by the measurement of coincidences between α particles and γ rays. While the Q_α of 4012(10) keV and half–life of 3.1(0.1) ms for the ground–state–to–ground–state decay of ^{107}Te had been known from previous work, Seweryniak et al.

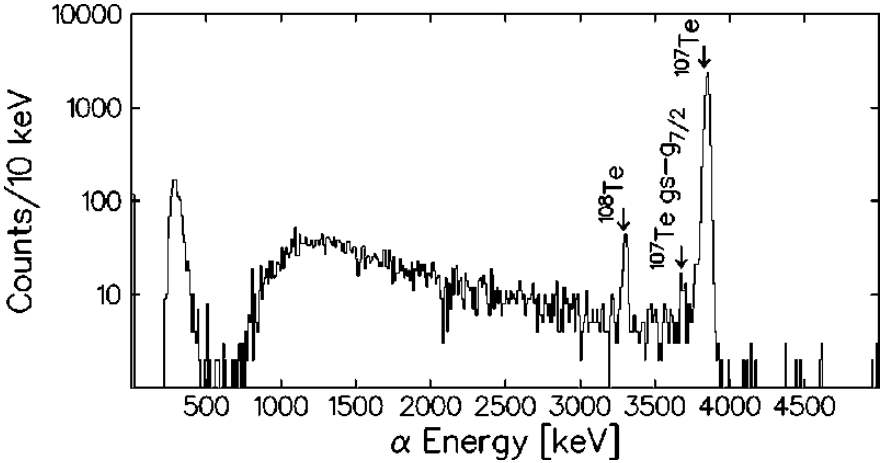

Fig. 8. Energy spectrum of α particles, measured for the decay of ^{107}Te [87]

succeeded for the first time to identify a fine–structure effect in α decay of nuclei northeast of ^{100}Sn. Their finding lead to assigning, in agreement with results obtained in earlier in–beam experiments, the 168 keV state to be the first excited $\nu g_{7/2}$ single–particle state in ^{103}Sn. The resulting W_α values are 2.0 for the ground–state–to–ground–state and 0.15 for the fine–structure transition. While the former agrees with what is expected from the above-mentioned systematics for 0^+ to 0^+ decays, the latter is so low that it was used [87] for interpreting of the structure of the $(\nu d_{5/2})$ ^{107}Te parent–state on the basis shell–model considerations. This interpretation neglects the process of α–particle formation and is thus of qualitative nature only.

It is interesting to speculate whether fine–structure studies can be extended to trans–^{100}Sn nuclei further away from the β–stability line, e.g to ^{105}Te. Such a measurement seems to be feasible, even though difficult. The experimental problems are related to the small production cross–section expected (10 nb for the ^{54}Fe(^{58}Ni,α3n) reaction) and to the short half–life of 1 μs or lower, estimated for this nucleus on the basis of the Gamow theory (see Sect. 2.2) and Q_α and W_α systematics. However, the determination of the hitherto unknown excitation energy of the $\nu g_{7/2}$ single–particle state in ^{101}Sn certainly justifies a special experimental effort which would allow one to perform a stringent test of shell–model predictions near ^{100}Sn.

6.2 Experiments on Direct One–Proton Radioactivity

The bulk of the experimental data on direct one–proton radioactivity has been gained by studying the odd-Z isotopes between thulium (Z=69) and iridium (Z=77). Figure 5 of [21] gives an overview of the 1997 status of this research by marking in a section of the nuclidic chart the experimen-

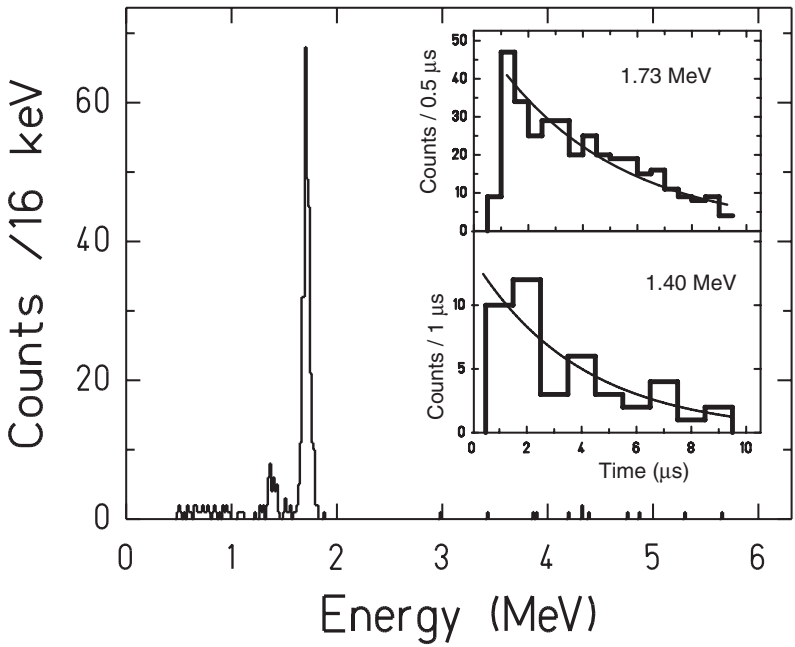

Fig. 9. Energy spectrum of protons, measured for the decay of ^{145}Tm [88]

tally identified cases of direct one-proton radioactivity as well as predictions of the one-proton drip line and of the ground–state deformations. As can be seen from this figure, this disintegration mode has been identified for at least two isotopes of the elements from thulium to iridium (The fact that odd-Z emitters prevail is due to the pairing effect of the mass–energy surface, as already mentioned in Sect. 2.2). With some 40 cases studied to date, the direct proton radioactivity has meanwhile been exploited as an almost standard spectroscopic tool for investigating N≃Z nuclei (see [21,85] for recent reviews). As was mentioned in Sect. 2.2, a spectroscopic factor of the oredr unity is found for, e.g., ^{145}Tm and ^{151}Lu by using a sperical potential within the Gamow approach. However, the spectroscopic factors determined for other proton emitters can not be interpreted in such a straightforward manner. Like in the case of α decay, one may hope to get a deeper insight by studying fine–structure phenomena.

An example for such a study is the recent experiment on ^{145}Tm, performed by Karny et al. [88] at the Recoil Mass Separator of the Oak Ridge National Laboratory. The proton spectrum obtained for the decay of this short-lived ($T_{1/2} = 3.1(0.3)\mu s$) nucleus is displayed in Fig. 9. Very much like in the case of the α–decay fine structure of ^{107}Te, discussed in Sect. 6.1, the Q value of 1728(10) keV for the ground–state to ground–state decay was already known from previous work. The new result obtained by Karny et al. concerns a

9.6(1.5) % branch to the first excited 2^+, 330(10) keV state in ^{144}Eu, which had remained unobserved previously. This finding yields, on the basis of a model calculation assuming a quadrupole deformation parameter β_2 of 0.18, quantitative information on the wave–function of the proton–emitting ^{145}Tm state.

6.3 Discovery of Direct Two–Proton Radioactivity

It is clear that, due to the short half–lives expected for direct two–proton emitters (see Sect. 2.2), the search for this disintegration mode is a domain of in-flight separators. It were indeed experiments performed at such facilities, namely the FRS of GSI Darmstadt and the the LISE3 of GANIL, which allowed for the first time to observe direct two–proton emission, the sixth form of radioactivity in addition to alpha, beta, gamma, fission and one-proton decay.

The results obtained by the two experiments [89,29] are shown in Fig. 10. Both of them used the fragmentation of a ^{58}Ni beam to produce ^{45}Fe, implanted the latter ions into a stack of Si detectors, and studied their decay. On the basis of time correlation measured in the two experiments, the half–life of ^{45}Fe was deduced to be $3.8^{+2.0}_{-0.8}$ ms. Moreover, by evaluating anti–coincidence relations with positrons [29] or annihilation radiation [89] it was assured that the 1.1 MeV events do *not* represent β-delayed particles. For all theses events the two protons were not recorded separately but together as one event. Hence, the type of particle has not been identified and there is no experimental proof of the emission of two particles. However, the interpretation as direct two–proton emission is the most obvious explanation of the phenomena observed. It remains a task for future experiments to determine the correlation of the protons in energy and angle and thus to clarify the type of emission process (see Sect. 2.2).

7 Experiments on β Decay

7.1 Precision Studies of 0^+ to 0^+ Fermi β Decay: The Link to Fundamental Physics

The CVC hypothesis together with the nine most precisely measured for the 0^+ to 0^+ Fermi β decays of ^{10}C to ^{54}Co, mentioned in Sect. 2.3, yield an average $\mathcal{F}t$ value of 3072.2(8) s [39]. This probably represents the most accurate quantity measured in nuclear physics to date. It should be noted that the precision of 2 parts in 10^4 reached for this quantity has required to measure the half–life, branching ratio and Q_{EC} value for these none decay to be better than a few parts in 10^4, corresponding to precisions between x and y parts in 10^4 for the nine individual Ft values.

The coupling constant G_F together with the coupling constant for muon decay allows to determine the V_{ud} matrix element of the Cabbibo-Kobayashi-Maskawa (CKM) quark mixing matrix, which in turn can be used to study

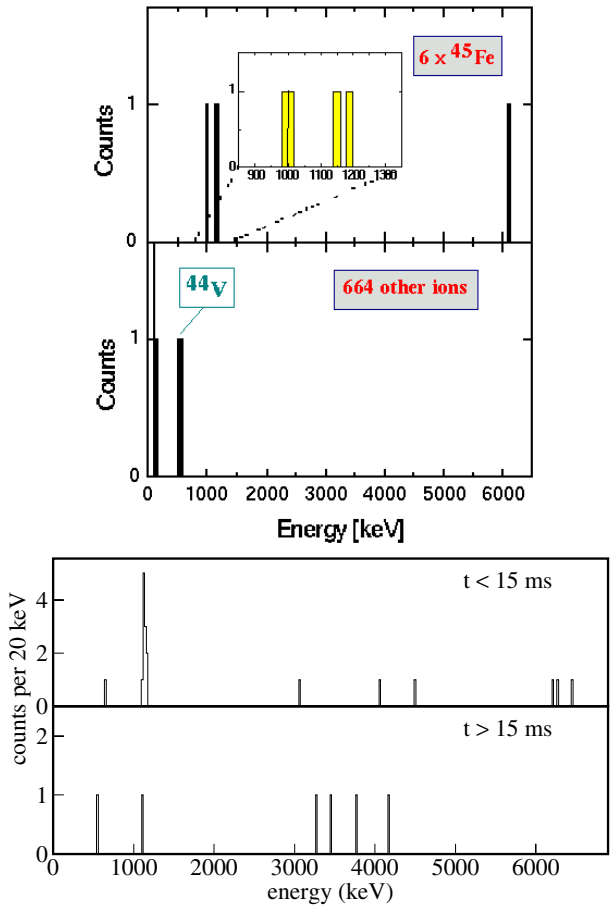

Fig. 10. Decay energy spectra measured for the decay of ^{45}Fe at GSI [89] (upper two panels) and GANIL [29] (lower two panels). The energy release of 1.1(1) MeV for four events observed at GSI (first panel from above) agrees with the result of 1.14(5) MeV obtained on the basis of 14 events at GANIL (third panel from above). The coincidence time windows following the implantation of the ions were chosen to be 10 and 15 ms, and the total counting times amounted to 6 d and 36 h, respectively. The second and fourth panel from above show background spectra which were generated by demanding coincidence with other ions than ^{45}Fe in the former and by extending the coincidence time to values above 15 ms in the latter case. In the GSI experiment, four of the five ^{45}Fe decay–events identified are assigned to direct two–proton emission, while the 6 MeV energy–loss event is interpreted as β-delayed proton decay of this nucleus (first panel from above); the 0.6 MeV event observed in the decays of the 664 other ions probably represents the energy loss of a β-delayed α particle from the decay of ^{44}V (second panel from above)

the unitarity of the CKM matrix. This question has attracted much interest in recent years, as there are indications that the top row of the CKM matrix is not unitary. The result deduced on the basis of Ft data for the sum of the elements in the first row is 0.9968(14), hence deviates from unity at the 2.2 σ level [39,40]. The most recent measurement of the neutron β–decay asymmetry [43] yields an even lower value of the unitarity sum. However, a recent measurement [90] of the $K^+ \rightarrow \pi^0 e^+ \nu$ decay indicates that the previously accepted value of V_{us} might be too low. The new value of V_{us}, if confirmed, would restore unitarity of the first row of the CKM matrix (0.9999(16) instead of 0.9968(14) before). A deviation from unitarity would have far reaching consequences for the standard model of the weak interaction and would point to physics beyond the currently accepted model.

Before the existence of physics beyond the standard model can be advocated, the different inputs into the determination of the corrected Ft value which leads to the calculation of the CKM matrix element should be carefully checked. It has turned out that the main uncertainty for the value of the V_{ud} matrix element comes from theoretical uncertainties linked to the different correction factors. The calculated terms $\delta_R^{'}$ and Δ_R^V are of the order 1.5 % and 2.4 %, respectively, while $\delta_C - \delta_{NS}$ varies between 0.26(2) % and 0.72(5) % for the nine well-studied decays with 10≤A≤54 (see (8) for the definition of these parameters). The influence of the correction can, e.g., be seen from Fig. 1 of [39]. However, for heavier 0^+ to 0^+ β decays, $\delta_C - \delta_{NS}$ increases being, e.g., 1.5(4) % for ^{74}Rb. Therefore, precise measurements of 0^+ to 0^+ transitions in A≥62 emitters would provide an important test of theoretical calculations of analog–symmetry breaking.

Based on these considerations, recent measurements of the half–lives, β–decay branching ratios and Q_{EC} values have been performed for A≥62 nuclei. Some of the corresponding experiments are of exploratory character [75,77, 78] rather than intended to yield results of the high accuracy required in this context. However, data of the latter sort were recently obtained for ^{62}Ga and ^{74}Rb at ISOL facilities (GSI–ISOL, IGISOL, ISAC, ISOLDE) and at the Magnetic Recoil Separator of Texas A&M University. These data will be briefly listed in the following:

- The half–lives of ^{62}Ga [91,92] and ^{74}Rb [94,93] were determined with precisions reaching a few parts in 10^5.
- The branching ratio of the super-allowed 0^+ to 0^+ transition to the ground state of the daughter nucleus is determined by subtracting the non-superal-lowed β feeding to excited states from the total intensity of the decay. This is a formidable task as for A≥62 nuclei an abundant number of (high-lying) 1^+ and 0^+ states is expected to be (weakly) populated by GT and nonanalog Fermi transitions [97]. Attempts to tackle this pandemonium problem (see Sect. 2.3) by high–resolution spectroscopy have been undertaken for ^{62}Ga [38,95,96] and ^{74}Rb [94,98,99]. A new approach was recently suggested by Piechaczek et al. [98]. These authors measured

β intensities for low-lying ^{74}Kr levels and used a comparison between the experimental findings and the corresponding shell–model predictions to adjust the calculation. In this way, they estimated the total branching ratio for non-superallowed β decays of ^{74}Rb to be 0.5(1) %. Thus, the branching ratio of the superallowed Fermi transition was found to be 99.5(1) %, representing a precision of one part in 10^3. It is interesting to note that this study of low-lying ^{74}Kr states is also related to the investigation of the isomer in this nucleus, discussed in Sect. 9.1.

- The mass of ^{74}Rb was determined with an accuracy of 18 keV, corresponding to two parts in 10^7 [100]. Together with the even more accurately determined mass of ^{74}Kr, the Q_{EC} value of ^{74}Rb has thus been determined with an accuracy of two parts in 10^3. This result, obtained for a truly exotic nucleus, is indeed impressive. However, due to the 5th power dependence of f upon the Q value, the corresponding precision in f is only 1 %.

In summarizing the new data for 0^+ to 0^+ Fermi decays of A≥62 nuclei, it seems as if ^{74}Rb plays a key role. Once its Q_{EC} and f value could be improved by a factor of about four, this result together with the above-mentioned half–life and branching–ratio data would allow one to perform a meaningful test of both the $\delta_C - \delta_{NS}$ correction for A=74 and thus a correspondingly enlarged test of the CVC hypothesis [6]. Such a measurement is underway, with the accuracy of the ^{74}Rb Q_{EC}–value probably reaching a precision of five parts in 10^4 [101] (see also [4,6]). Thus, a crucial test of the theoretical $\delta_C - \delta_{NS}$ correction–term of 1.5(4) % for ^{74}Rb will be feasible soon.

7.2 Beta Decay near ^{100}Sn: Observation of the GT Resonance

As already mentioned in Sect. 2.3, β–decay studies of nuclei below ^{100}Sn offer the chance to observe the entire GT resonance. Based on this motivation, several such decays, namely those of ^{97}Ag [102], a three proton–hole nucleus with respect to ^{100}Sn, as well as ^{98}Ag [103] and ^{102}In [104] were investigated at the GSI–ISOL facility by using both the Cluster Cube and the TAS (see Sects. 3.3 and 3.4). Figure 11 displays the experimental results obtained for ^{98}Ag from the two different techniques. The most striking result of these measurements is that the Cluster Cube, even though being probably the most advanced high–resolution detectors for β-delayed γ rays available to date, missed about 30 % of the β intensity recorded by the TAS (see Fig. 11). For the case of ^{97}Ag this difference is much smaller about 9 %. However, the missing fraction of the ΣB_{GT} value, defined in Sect. 2.3, amounts still to about 21 % for ^{97}Ag. For the case of ^{102}In, the Cluster Cube data miss the GT resonance almost entirely.

As can be clearly seen from Fig. 12, the TAS data have allowed one to unambiguously identified GT resonance for the ^{97}Ag decay: The distribution of the GT strength as a function of the ^{97}Pd excitation energy, deduced from

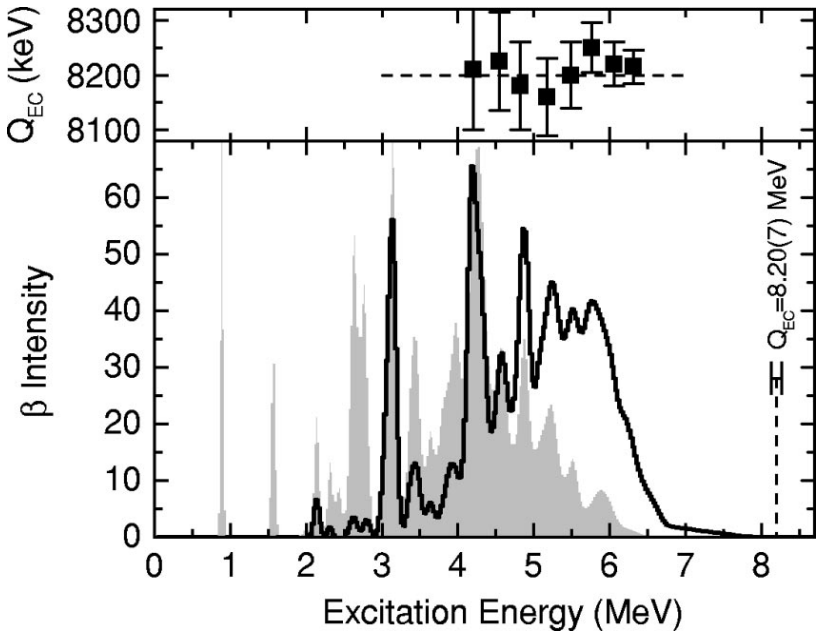

Fig. 11. Lower panel: β-intensity distribution for the ^{98}Ag decay, obtained by using the TAS (solid–line curve) and the Cluster Cube data (shaded area). The experimental Q_{EC} value is indicated by an vertical dashed line. Upper panel: Q_{EC} values (squares) obtained by using the experimental EC/β^+ ratios which were deduced for selected ^{98}Pd excitation–energies. The weighted average of 8.20(7) MeV obtained for the Q_{EC} value is indicated by a horizontal dashed line [103]

the TAS data, shows a pronounced resonance at an energy around 6 MeV with a width of about 1 MeV. The shape of the GT resonance agrees qualitatively with that obtained by a shell–model calculation which uses the SNB hamiltonian [83,102] and a model space in the active protons are restricted to the $1p_{1/2}$ and $0g_{9/2}$ orbitals, the $1p_{1/2}$ and $0g_{9/2}$ orbitals for neutrons are always filled and the active neutrons are restricted to the $0g_{7/2}$, $1d_{5/2}$, $1d_{3/2}$, $1s_{1/2}$ and $0h_{11/2}$ orbitals. The ΣB_{GT} values of ^{97}Ag are 3.0(4) from the experiment, and 12.88 from the SNB model. In the latter case, the SNB result for $N_{9/2}$ is used in (3). The resulting hindrance factor for ΣB_{GT} amounts to 4.3(6) with reference to the SNB calculation, which agrees with the value of 3.7 expected from further configuration mixing within the SNB model space and from the higher–order configuration mixing beyond that space (see [83, 102] for details).

Further TAS data have been obtained for ^{100}In [120], $^{103-107}$In [105,106] and, most recently for ^{102}Sn [59,60]. These data, together with those for ^{97}Ag [102] and ^{98}Ag [103], discussed above, as well as ^{98}Cd [107] can now be used to establish for the first time a mass dependence of the GT hindrance

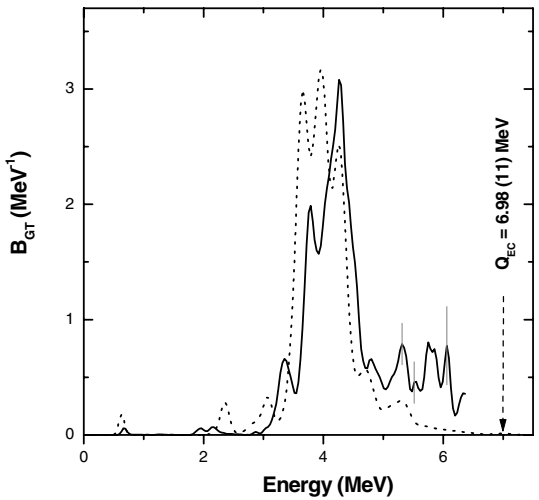

Fig. 12. Gamow-Teller strength for the β decay of ^{97}Ag, deduced from the TAS data (dashed–line histogram) and from the SNB shell-model calculation (solid–line histogram). The theoretical GT strength distribution was adapted to the TAS resolution by a smoothing procedure and reduced by a hindrance factor 4.3 (see text). The experimental Q_{EC} value is indicated by an arrow [102]

factor near ^{100}Sn. As far as the properties of for this truly exotic nucleus are concerned, the few events observed so far were sufficient for unambiguous Z and N identification [108,109], half-life ($1.0^{+0.6}_{-0.3}$ s) [110] and mass [111] determination. However, more detailed spectroscopic data are missing and, in particular, the super GT resonance, expected for the decay of ^{100}Sn (see Sect. 2.3), still awaits experimental confirmation.

7.3 Beta-Delayed Proton Emission of ^{57}Zn

The β-delayed proton emission in the decay of ^{57}Zn ($T_{1/2}$ = 38(4) ms, $I^\pi = 7/2^-$, $T_z = -3/2$, T = 3/2) [58] may serve as a first example for illustrating the main features of this disintegration mode (Another example will be discussed in Sect. 9.2). The proton energy spectrum, measured for this decay at the GSI–ISOL facility, is displayed in Fig. 13. The decay of ^{57}Zn is characterized by the competition of Fermi and GT transitions. This situation was sketched in Fig. 3 and is similar to that occurring for the case of ^{33}Ar that was briefly mentioned in Sect. 2.3 (cf. Fig. 4). However, contrary to the latter case, the experimental energy resolution of 30 keV FWHM, even though being state–of–the–art for such measurements, does not allow one to trace recoil–broadening effects in a singles spectrum.

Two observations can be readily made by inspecting these data. Firstly, a dominant part of the proton intensity stem from the $I^\pi = 7/2^-, T = 3/2$ isobaric analog state (IAS) in ^{57}Cu, leading to the 1902 and 4595 keV proton

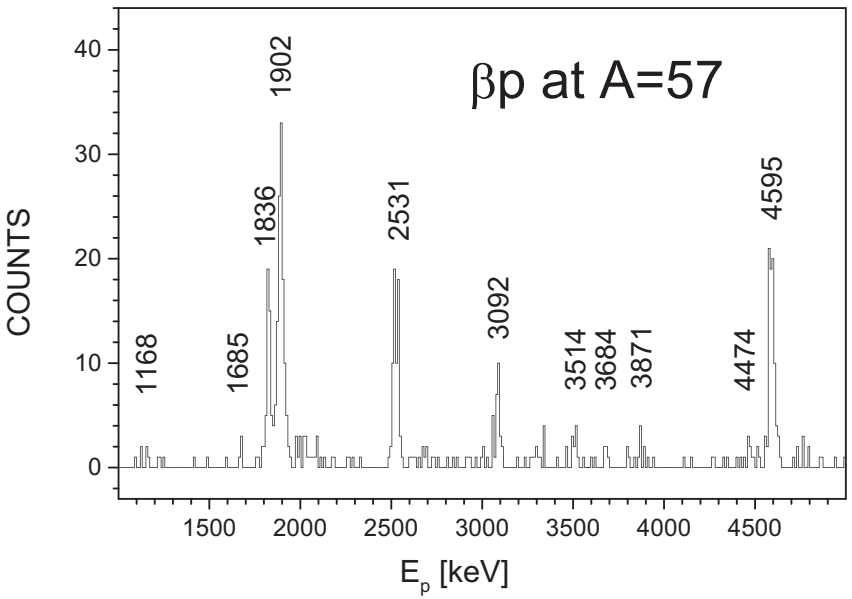

Fig. 13. Energy spectrum of β-delayed protons, measured for the decay of ^{57}Zn. Prominent proton lines are marked by their centre–of–mass energies. The 1902 and 4595 keV lines correspond to proton emission from the IAS in ^{57}Cu to the first excited 2^+ level and the 0^+ ground–state of ^{56}Ni, respectively. Thus, the energy difference between these two lines correspond to the (known) excitation energy of the first 2^+ level of the doubly magic nucleus ^{56}Ni [58]

lines that can be seen from Fig. 13. This dominance reflects the larger matrix element of the Fermi β transition compared to those of ordinary allowed (GT) ones. The latter contributes to a lesser but still sizeable amount to the proton intensity, as can be seen from Fig. 13 by taking those lines into account that are not attributed to the IAS decay.

The second feature that is apparent in Fig. 13 concerns the fact that the intensity of the proton transition from the IAS in ^{57}Cu to the first excited 2^+ of ^{56}Ni is *larger* than that of the corresponding transition to 0^+ ground–state of ^{56}Ni. This is in striking contrast to the low relative intensity of fine–structure lines in direct α and proton decay, discussed in Sects. 6.1 and 6.2. Taking into account that the latter charged–particle transitions are isospin allowed, the anomalous fine–structure intensity observed in the IAS–related proton emission can be qualitatively interpreted as an isospin–mixing effect. The corresponding shell–model filling diagram is shown in Fig. 14.

The ground state of ^{57}Zn is described as a $[(\pi p_{3/2})^2(\nu f_{7/2})^{-1}]_{7/2^-,T=3/2}$ configuration. Its Fermi β–decay involves either one of the (eight) protons from the (completely filled) $f_{7/2}$ orbital or one of the (two) $p_{3/2}$ protons. The two disintegration modes populate two different $7/2^-, T = 3/2$ (three–

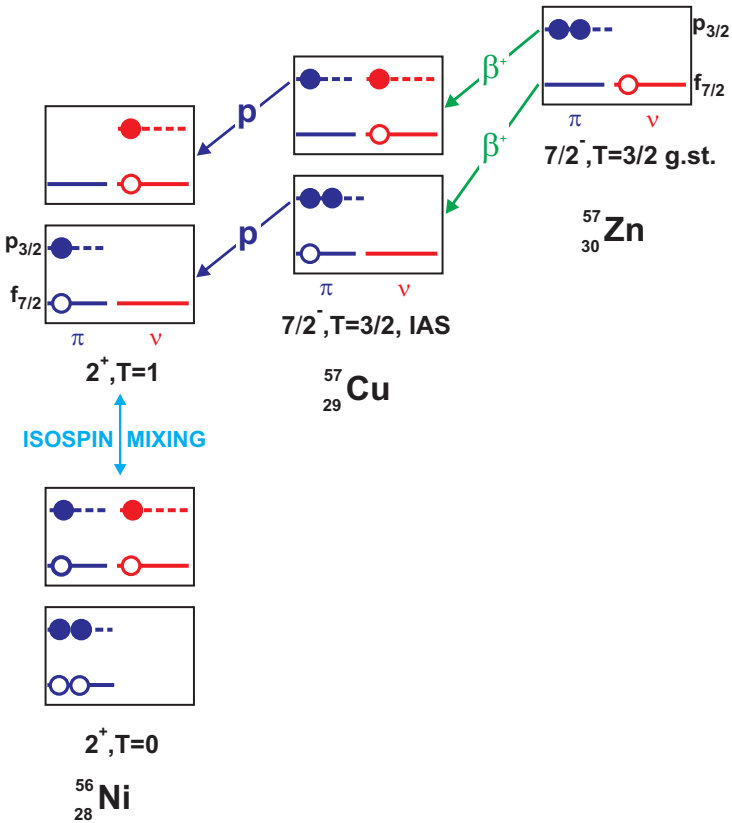

Fig. 14. Shell–model filling diagram used to interpret the anomalous fine–structure intensity, observed for proton emission from the IAS in ^{57}Cu. For simplicity, only transitions leading to 2^+ states in ^{56}Ni are shown. See text for details

quasiparticle) configurations of the IAS state in the intermediate nucleus ^{57}Cu. The subsequent proton emission from the IAS yields in turn two different $2^+, T = 1$ (two–quasiparticle) states in the final nucleus ^{56}Ni, namely a $(\pi f_{7/2})^{-1}\pi p_{3/2}$ and a $(\nu f_{7/2})^{-1}\nu p_{3/2}$ one. What is finally observed in the experiment, however, are *not* the proton transitions to these high-lying T=1 states of ^{56}Ni but rather to its low-lying $2^+, T = 1$ and $0^+, T = 1$ levels. Even though isospin–mixing *matrix elements* are expected to be small, the isospin–forbidden transition to the latter states dominate the IAS decay due to the energy (and angular–momentum) dependence of the barrier-transmission probability (see Sect. 2.2).

8 Experiments on γ-Delayed Charged–Particle Emission: A Novel Tool of In–Beam Spectroscopy

The 'traditional' method of in–beam spectroscopy is based on studying γ–ray and conversion electrons emitted from highly excited high–spin states populated in nuclear reactions (see [5] and Sect. 9.1). In recent years, this method has been enriched by a new and exciting facet, i.e. the detection of γ-delayed charged particles (see [112] for a review). The lifetimes of the proton–emitting states are generally below the limit of 20 ns, assumed in the definition of term 'decay' (see Sect. 2.2). Nevertheless, this disintegration mode will be briefly discussed here due to its similarity with direct and β-delayed proton emission.

The example selected here concerns in–beam studies of ^{58}Cu and ^{57}Ni, hence involving nuclei near ^{56}Ni similar to those studied in the ^{57}Zn decay discussed in Sect. 7.3. The measurements were performed by using modern Ge–detector arrays for γ–ray spectroscopy but, in contrast to most of the experiments described in Sects. 6 to 7.3 and Sect. 9.2 and similar to those presented in Sect. 9.1, did *not* involve any magnetic separation of the reaction residues.

The main experimental results obtained by in–beam spectroscopy of ^{58}Cu are sketched in Fig. 15. While the *spherical* states of ^{58}Cu have been solely identified by measuring γ–ray transitions, the *deformed* levels in this nucleus were studied by detecting both γ rays and protons. The yrast cascade connecting the deformed levels was identified by observing electromagnetic transitions all the way down to a 8915 keV, (9^+) state whose spin is apparently low enough to make proton emission to the 3701 keV, $9/2^+$ state in ^{57}Ni a competitive disintegration mode. The energies given here correspond to ex-

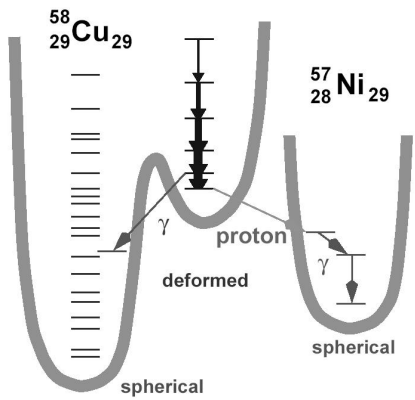

Fig. 15. Sketch of the process of γ-delayed proton emission for the case of ^{58}Cu→^{57}Ni [112]

citation energies with reference to the ground state of the respective nucleus. This means that the above-mentioned proton transition has a center–of–mass energy of about 2300 keV, taking the known proton–separation energy in ^{58}Cu into account.

All in all, the novel technique of detecting γ-delayed charged-particle emission holds great promise. For the case of ^{58}Cu it was possible to, e.g., tentatively make spin and parity assignments to the deformed states in ^{58}Cu as well as to excited levels of ^{57}Ni, and to deduce the lifetime of the proton emitting 8915 keV state to be in the range from 0.1 to 0.6 ps. It seems clear that this method will become even more powerful for in–beam studies of nuclei that are closer or even beyond the N=Z line and have thus lower thresholds for charged–particle emission.

9 Isomer Spectroscopy

9.1 Shape Isomer in ^{74}Kr

Theoretical model calculations predict that nuclei with N,Z = 30 – 40 exhibit a variety of different shapes. This feature can be experimentally probed, e.g., by investigating the low-lying, isomeric 0^+ states of even-even krypton isotopes. In–beam measurements show that highly excited, high–spin states of ^{74}Kr have properties of a well-deformed rotor [113]. The first excited 0^+ state in this nucleus was found to be an isomer. This result was first obtained in a GANIL experiment using ^{92}Mo fragmentation [114], follow-up experiments were performed at IReS Strasbourg with ^{58}Ni(^{19}F,p2n) fusion–evaporation reactions [115] and at GANIL again by means of ^{78}Kr fragmentation [116]. In the latter two measurements both γ–rays and conversion electrons were detected.

The spectra obtained in the Strasbourg experiment, together with the scheme of low-lying ^{74}Kr levels, is displayed in (Fig. 16).

The partial level scheme, deduced from these data, includes two high-lying (2^+) states and the isomeric 0^+ state at 508 keV which de-excites through an E0 transition to the ground state and an 52 keV E2 transition to the 2^+ state at 456 keV. The half–life of 18.8(1.0) ns [116] measured for the isomer together with the intensity ratio between the E0 and E2 transition allow one to determine the E0 strength. On the basis of a two-level mixing model, strong mixing has been deduced between oblate 0^+ ground–state and the prolate first-excited 0^+state [115].

In concluding this chapter, two general comments will be made. Firstly, in–beam and isomer–decay spectroscopy of states in even-even T_z=1 nuclei are strongly related to precision studies of superallowed Fermi transitions, as may be seen from the ^{74}Rb $\rightarrow$ ^{74}Kr decay (see Sect. 7.1). Secondly, if an isomeric nuclear state disintegrates (partly) by EC decay or converted transitions its lifetime depends on the atomic charge state of the atom. This effect, which reminds one of the bound–state β decay of highly stripped ions [3],

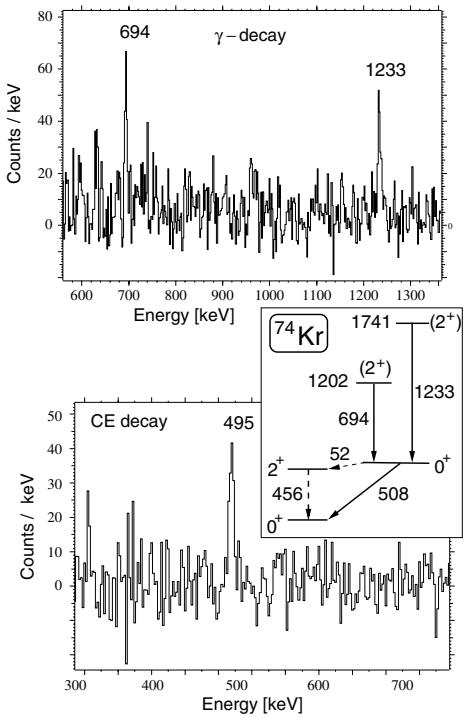

Fig. 16. Gamma–ray and conversion–electron data obtained for transitions in ^{74}Kr: Gamma–ray spectrum taken in coincidence with the 495 keV conversion–electron line (upper panel), conversion–electron spectrum taken in coincidence with the 694 and 1233 keV γ–ray lines (lower panel), and partial level scheme of ^{74}Kr, deduced from these data (central panel) [115]

may also be of astrophysical interest. The role of ^{80m}Y for the *rp* process can be taken as an example [117].

9.2 Spin–Gap Isomer in ^{94}Ag

Spin–gap isomers, also called yrast traps, occur for N≤Z isotopes of palladium, silver and cadmium (see [1] for the shell–model interpretation of this phenomenon). Several of them have been experimentally identified recently. Here, ^{94}Ag is taken as an example. All measurements on isomerism in this nucleus have been performed at the GSI–ISOL facility by using ^{58}Ni(^{40}Ca,p3n) reactions. By studying β-delayed protons, a 0.42(5) s isomer in this nucleus was observed [118]. Subsequent measurements of β-delayed γ–rays [119,120] and protons [67] have yielded evidence for the existence of an additional isomer of comparable half–life. The up-to-date experimental results, obtained from these works for the decay properties of the two isomers, are sketched in Fig. 17.

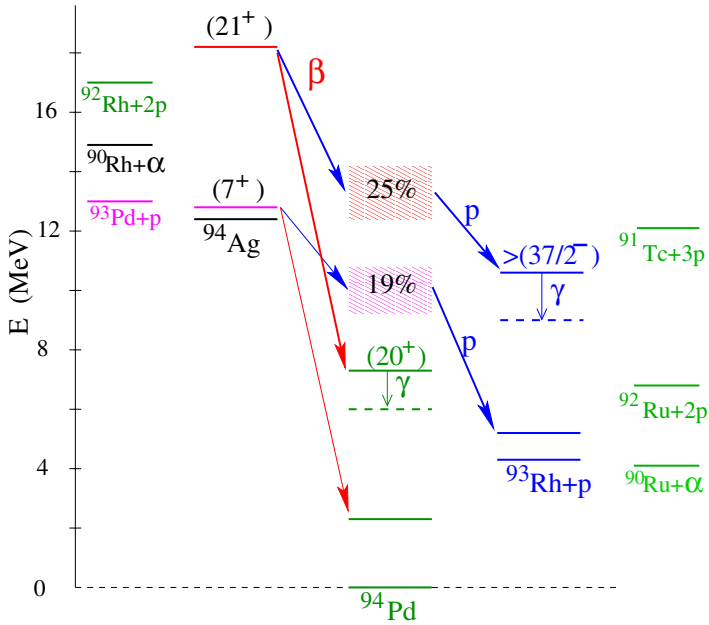

Fig. 17. Decay scheme of the (7^+) and (21^+) isomers of ^{94}Ag. In addition to the β-delayed γ and proton branches, thresholds are given as estimated [10] for α, proton and two–proton emission from ^{94}Ag (leftmost panel) and proton and two–proton emission from ^{94}Pd (rightmost panel) [67]

The β-delayed proton decay mode, having branching ratios of 19 and 25 %, yields half–life values of 0.62(3) and 0.42(5) s for (7^+) and (21^+) isomer, respectively. On the basis of shell–model calculations, the occurrence of spin–gap isomerism is interpreted as being due to the large spin difference between the first excited 7^+ level and the 0^+ ground-state, and by the inversion between 19^+ and 21^+ levels, respectively. From these calculations, the excitation energy is predicted to be 0.7 and 6.3 MeV, respectively. The isomers decay by β-delayed γ–ray emission to ^{94}Pd states with spin values up to 20, and by β-delayed proton emission to ^{93}Rh states with spin values up to 39/2 or more. Thus, one may call this studies 'high–spin decay spectroscopy', the spin values involved being considerably above those observed in γ-delayed proton emission (see Sect. 8).

A detailed comparison between experimental ^{94}Ag and ^{94}Pd level energies and the corresponding shell–model predictions is given in [1]. As shown there, the inversion of the 19^+ and 21^+ levels is reproduced only if one uses a large–scale shell–model calculation that is performed in a *gds* space and allows up to four–particle/four–hole excitations across the ^{100}Sn shell–closure.

The (21^+) isomer in ^{94}Ag is a truly exotic nuclear state with respect to its high–spin, high excitation energy and long β–decay half–life, the combina-

tion of these properties being unprecedented on the entire chart of nuclides. As indicated in Fig. 17 by the respective thresholds, the (21^+) isomer is unbound against α, proton and two–proton emission, while for both isomers β-delayed two–proton and two–proton decay is energetically possible. However, the thresholds are defined with respect to the *ground states* of the daughter nuclei populated by the emission whereas the high spin of the parent state requires, due to the centrifugal barrier (see Sect. 2.2), a comparatively high spin of the daughter state. As the latter levels have large excitation energies, the effective Q values for the decays are reduced and their observation is probably a difficult task.

Another interesting feature is that the superallowed Fermi decay of the 0^+ ground–state of ^{94}Ag, with a half–life of 29^{+29}_{-10} ms [77], has not been observed in these experiments. This is apparently related to the fact that the heavy–ion induced fusion–evaporation reactions such as ^{58}Ni(^{40}Ca,p3n) preferably populate high–spin states. Correspondingly, the (7^+) and (21^+) isomers receive the major share of the ^{58}Ni(^{40}Ca,p3n) cross–section and, in the absence of major internal branches of their de–excitation, 'block' the population of the ground–state in this reaction. Contributions of the ground–state of ^{94}Ag to the mass–separated A=94 beam are further suppressed due to the delay occurring in ISOL ion–sources.

10 Summary and Outlook

This lecture on decay properties of N≃Z nuclei dealt with a rapidly developing research field. A number of exciting new results were presented, such as the first observation of the two–proton radioactivity and the new experimental methods of studying γ-delayed charged–particle emission (from ^{58}Cu), performing high–spin decay spectroscopy (of ^{94m}Ag) and approaching ^{100}Sn in decay spectroscopy. Moreover, this lecture outlined a few challenges, namely

- clarifying the two–proton decay mode (when searching for this disintegration mode for ^{48}Ni, the heaviest nucleus is involved in which isospin symmetry can be studied in comparison to its mirror, ^{48}Ca),
- extending the precision measurements of 0^+ to 0^+ Fermi decays to A≥62 nuclei,
- probing the super GT resonance of ^{100}Sn, and
- searching for signatures of neutron–proton pairing.

This list has every chance to be incomplete as one should be ready for surprises in this truly evolutionary field. All in all, it seems indeed justified to speak of the particular, multidisciplinary interest underlying the investigation of nuclei with equal or almost equal number of neutrons and protons.

Acknowledgement

After more than 27 years of on-line operation, the GSI–ISOL facility is being decommissioned these days. The author would like to take this occasion to acknowledge with pleasure the fruitful collaboration with the long–term companions of the GSI–ISOL Group, in particular K. Burkard, W. Hüller and R. Rirchner, as well as with many colleagues from GSI, the University of Warsaw and numerous other institutions around the world. The lecture presented here was partially supported by a Humboldt Honorary Fellowship of the Polish Science Foundation.

References

1. H. Grawe, Shell Model from a Practitioner's Point of View, Lect. Notes Phys. **651**, 33–75 (2004)
2. D.J. Morrissey, B.M. Sherrill, In-Flight Separation of Projectile Fragments, Lect. Notes Phys. **651**, 113–135 (2004)
3. F. Bosch, Measurement of Mass and Beta-Lifetime of Stored Exotic Nuclei, Lect. Notes Phys. **651**, 137–168 (2004)
4. G. Bollen, Traps for Rare Isotopes, Lect. Notes Phys. **651**, 169–210 (2004)
5. R. Julin, Gamma-Ray and Conversion-Electron Spectroscopy of Exotic Heavy Nuclei, Lect. Notes Phys. **651**, 263–294 (2004)
6. N. Severijns, Weak Interaction Studies by Precision Experiments in Nuclear Beta Decay, Lect. Notes Phys. **651**, 339–381 (2004)
7. K. Langanke, F.-K. Thielemann, M. Wiescher, Nuclear Astrophysics and Nuclei far from Stability, Lect. Notes Phys. **651**, 383–467 (2004)
8. G. Audi et al.: Nucl. Phys. A **729**, 3 (2003)
9. A. Wapstra, G. Audi, C. Thibault: Nucl. Phys. A **729**, 129 (2003)
10. G. Audi, A.H. Wapstra, C. Thibault: Nucl. Phys. A **729**, 337 (2003)
11. *http : //csnwww.in2p3.fr/AMDC/web/amdc*
12. J. Cerny, J.C. Hardy: Ann. Rev. Nucl. Part. Sci. **27**, 333 (1977)
13. O.V. Bochkarev et al.: Sov. J. Nucl. Phys. **55**, 955 (1992)
14. H.O.U. Fynbo et al.: Nucl. Phys. A **718**, 541 (2003)
15. E. Gete et al.: Phys. Rev. C **61**, 064310 (2000)
16. L. Buchmann, E. Gete, J.C. Cow, J.D. King, D.F. Measday: Phys. Rev. C **63**, 034303 (2001)
17. U.C. Bergmann et al.: Nucl. Phys. A **692**, 427 (2001)
18. Y. Prezado et al.: Phys. Lett. B **576**, 55 (2003)
19. J.O. Rasmussen: Phys. Rev. **113**, 1593 (1959)
20. E. Roeckl: 'Alpha Decay'. In: *Nuclear Decay Modes*, ed. by D.N. Poenaru (IOP Publishing, Bristol and Philadelphia 1996) pp. 237–274
21. P. J. Woods, C. N. Davids: Annu. Rev. Nucl. Part. Sci. **47**, 541 (1997).
22. P. de Marcillac et al.: Nature **422**, 876 (2003)
23. V. Goldanskii: Nucl. Phys. **19**, 482 (1960)
24. K.P. Jackson et al.: Phys. Lett. B **33**, 281 (1970)
25. S. Hofmann et al.. Z. Phys. A **305**, 111 (1982)
26. O. Klepper et al.: Z. Phys. A **305**, 125 (1982)

27. A. Azhari, R.A. Kryger, M. Thoenessen: Phys. Rev. C **58**, 2568 (1998)
28. M.D. Cable et al.: Phys. Rev. C **26**, 1778 (1982)
29. J. Giovinazzo et al.: Phys. Rev. Lett. **89**, 102501 (2002)
30. R. Barton et al.: Can. J. Phys. **41**, 2007 (1963)
31. J.C. Hardy, E. Hagberg: 'Beta-delayed Proton and Alpha Emission'. In: *Particle Emission from Nuclei, Vol. 3*, ed. by D. Poenaru, M. Ivacsu (Chemical Rubber Company, Boca Raton 1988) pp. 99–131
32. J. Äystö, J. Cerny: 'Proton–rich Nuclei'. In: *Treatise on Heavy–ion SciencePparticle Emission from Nuclei, Vol. 8*, ed. by D.A. Bromley (Plenum, New York 1989) pp. 207–258
33. B. Jonson, G. Nyman: 'Beta–delayed Particle Emission'. In: *Nuclear Decay Modes*, ed. by D.N. Poenaru (IOP Publishing, Bristol and Philadelphia 1996) pp. 102–142
34. J.C. Hardy et al.: Phys. Rev. Lett. **37**, 133 (1976)
35. D. Schardt, K. Riisager: Z. Phys. A **345**, 265 (1993)
36. E.G. Adelberger et al.: Phys. Rev. Lett. **83**, 1299 and 3101 (1999)
37. A. Garcia et al.: Hyp. Int. **129**, 237 (2000)
38. J. Döring et al: 'Beta-decay Study of the N=Z Odd-odd Nuclei ^{62}Ga and ^{70}Br'. In: *Proc. Intern. Workshop on Selected Topics of N=Z Nuclei (PINGST 2000), June 6–10, 2000*, ed. by D. Rudolph, M. Hellström (Div. of Cosmic and Subatomic Phys., Lund University, Div. of Mathematical Phys., Lund Inst. of Technology 2000), LUIP 0003, pp. 131–136
39. I.S. Towner, J.C. Hardy: Phys. Rev. C **66**, 035501 (2002)
40. J.C. Hardy et al.: Nucl. Phys. A **509**, 429 (1990)
41. E. Klempt et al.: Z. Phys. A **37**, 179 (1988)
42. S.J. Freedman: Comments Nucl. Part. Phys. **19**, 209 (1990)
43. H. Abele et al.: Phys. Rev. Lett. **88**, 211801 (2002)
44. P.J. Brussard, P.W.M. Glaudemans: *Shell Model Applications in Nuclear Spectroscopy* (North Holland, Amsterdam 1977), p. 259 and Table 12.2
45. J.C. Hardy et al.: Phys. Lett. B **71**, 307 (1977)
46. J. Fujita et al.: Eur. Phys. J. A **13**, 411 (2002); H. Fujita: 'Isospin Symmetry Structure of Spin-Isospin Excitations in A=58 Nuclei'. Ph D Thesis, Osaka University (2002), unpublished
47. B.A. Brown, K. Rykaczewski: Phys. Rev. C **50**, 2270 (1994)
48. T. Wakasa et al.: Phys. Rev. C **55**, 2909 (1997)
49. K. Yako et al.: 'Determination of the Gamow-Teller Quenching Factor via the ^{90}Zr(n,p) Reaction at 293 MeV'. In: *Proc. Intern. Symposium on Frontiers of Collective Morion (CM 2002), November 6–9, 2000*, ed. by H. Sagawa, H. Iwasaki (World Scientific, New Jersey 2003), pp. 118–123
50. K. Langanke, G. Martínez-Pinedo: Nucl. Phys. A **673**, 481 (2000)
51. A. Heger et al.: Phys. Rev. Lett. **86**, 1678 (2001)
52. H. Schatz et al.: Phys. Rep. **294**, 167 (1998)
53. E. Roeckl et al.: Nucl. Instr. and Meth. in Phys. Res. B **204**, 53 (2003)
54. R. Kirchner et al.: Nucl. Instr. and Meth. in Phys. Res. A **234**, 224 (1985)
55. R. Kirchner et al.: Nucl. Instr. and Meth. in Phys. Res. B **26**, 204 (1987)
56. R. Kirchner: Nucl. Instr. and Meth. in Phys. Res. A **292**, 203 (1990)
57. R. Kirchner: Nucl. Instr. and Meth. in Phys. Res. B **204**, 179 (2003)
58. A. Jokinen et al.: EPJdirect A **3**, 1 (2002)
59. M. Karny et al.: 'Beta Decay Studies of Neutron-deficient Sn Isotopes'. In: *GSI Sci. Rep. 2002*, p. 3

60. Z. Janas et al.: unpublished result from GSI Experiment U180
61. C. Mazzocchi et al.: Phys. Lett. B **532**, 29 (2002)
62. I. Mukha et al.: 'Silicon Strip Detector for Decay Studies of Exotic Nuclei at the FRS and ISOL Facilities'. In: *GSI Sci. Rep. 2002*, GSI Report 2003–1 (2003), p. 225
63. Z. Hu et al.: Nucl. Instr. and Meth. in Phys. Res. A **419**, 121 (1998)
64. M. Karny et al.: Nucl. Instr. Meth. B **126**, 320 (1997)
65. J.C. Hardy: private communication
66. L. Batist et al.: Nucl. Phys. A **720**, 245 (2003)
67. I Mukha et al.: 'Beta-delayed proton decay of a high-spin isomer of ^{94}Ag'. In: *Proc. 2nd Intern. Symposium on Proton–emitting Nuclei, PROCON 2003, Legnaro, 2003*, ed. by E. Maglione, F. Soramel, AIP Conf. Proc. **681**, (AIP, Melville, NY 2003), pp. 209–214, submitted to Phys. Rev. C
68. P.G. Hansen: private communication
69. J. Chaumont et al.: Phys. Lett. B **29**, 652 (1969)
70. H.–J. Kluge: 'Recent Progress in Precision Mass Measurements'. In: *Proc. Intern. Conf. on Exotic Nuclei and Atomic Masses (ENAM 95), June 19–23, 1995*, ed. by M. de Saint Simon, O. Sorlin (Editions Frontières, Gif–sur–Yvette 1995) pp. 3–12
71. H.L. Ravn et al.: J. Inorg. Nucl. Chem. **37**, 383 (1975)
72. J.M. D'Auria et al.: Phys. Lett. B **66**, 233 (1977)
73. R. Pfaff et al.: Phys. Rev. C **53**, 1753 (1996)
74. B. Blank et al.: Phys. Rev. Lett. **74**, 4611 (1995)
75. C. Longour et al.: Phys. Rev. Lett. **81**, 3337 (1998)
76. Z. Janas et al.: Phys. Rev. Lett. **82**, 295 (1999)
77. A. Stolz et al.: 'Decay Studies of the N≃Z Nuclei from ^{77}Y to ^{100}Sn'. In: *Proc. Intern. Workshop on Selected Topics of N=Z Nuclei (PINGST 2000), June 6–10, 2000*, ed. by D. Rudolph, M. Hellström (Div. of Cosmic and Subatomic Phys., Lund University, Div. of Mathematical Phys., Lund Inst. of Technology 2000), LUIP 0003, pp. 113–117
78. J. Garcés Narro et al.: Phys. Rev. C **63**, 044307 (2001)
79. M.J. López Jiménez et al.: Phys. Rev. C **66**, 025803 (2002)
80. D. Lunney, J.M. Pearson, C. Thibault: Rev. Mod. Phys. **75**, 1021 (2003)
81. W. Satula, D.J. Dean, J. Gary, S. Mizutori, W. Nazarewicz: Phys. Lett. B **407**, 103 (1997)
82. B.A. Brown et al.: Phys. Rev. C **65**, 045802 (2002)
83. J. Britz, A. Pape, M.S. Antony: At. Data Nucl. Data Tables **69**, 125 (1998)
84. K. Blaum et al.: Phys. Rev. Lett. **91**, 260801 (2003)
85. K.P. Rykaczewski: Eur. Phys. J. A **15**, 81 (2002)
86. D. Schardt et al.: Nucl. Phys. A **368**, 153 (1981)
87. D. Seweryniak et al.: Phys. Rev. C **66**, 051307(R) (2002)
88. M. Karny et al.: Phys. Rev. Lett. **90**, 012502 (2003)
89. M. Pfützner et al.: Eur. Phys. J. A **14**, 279 (2002)
90. A. Sher et al.: Phys. Rev. Lett. **91**, 261802 (2003)
91. B.C. Hyman et al.: Phys. Rev. C **68**, 015502 (2004)
92. B. Blank et al.: Phys. Rev. C **69**, 015501 (2003)
93. G.C. Ball et al.: Phys. Rev. Lett. **86**, 1454 (2001)
94. M. Oinonen et al.: Phys. Lett. B **511**, 145 (2002)

95. J. Döring et al: 'β Decay of the Nuclei ^{60}Ga (T_z=-1), ^{62}Ga and ^{70}Br (T_z=0)'. In: *Proc. Intern. Conf. on Exotic Nuclei and Atomic Masses (ENAM 2001), July 2–7, 2001*, ed. by J. Äystö, P. Dendooven, A. Jokinen, M. Leino (Springer, Berlin, Heidelberg, New York 2003) p. 323
96. B. Blank et al.: Eur. Phys. J. A **15**, 121 (2002)
97. J.C. Hardy, I.S. Towner: Phys. Rev. Lett. **88**, 252501 (2002)
98. A. Piechaczek et al.: Phys. Rev. C **67**, 051305(R) (2003)
99. J. Huikari: 'ISOL-Method in Studies of Medium-heavy Z∼N Nuclei'. Ph D Thesis, University of Jyväskylä (2003), unpublished
100. F. Herfurth et al.: Eur. Phys. J. A **15**, 17 (2002)
101. A. Kellerbauer: private communication; D. Rodriguez: 'An RFQ Buncher for Accumulation and Cooling of Heavy Radionuclides at SHIPTRAP and High Precision Mass Measurements on Unstable Kr Isotopes'. Ph D Thesis, University of Valencia, GSI Rep. Diss. 2003-06 (2003)
102. Z. Hu et al.: Phys. Rev. C **60**, 024315 (1999)
103. Z. Hu et al.: Phys. Rev. C **62**, 064315 (2000)
104. M. Gierlik et al.: Nucl. Phys. A **724**, 313 (2003)
105. M. Karny et al.: Nucl. Phys. A **640**, 3 (1998)
106. M. Karny et al.: Nucl. Phys. A **690**, 367 (2001)
107. A. Płochocki et al.: Z. Phys. A **342**, 43 (1992)
108. R. Schneider et al.: Z. Phys. A **348**, 241 (1994)
109. M. Lewitowicz et al.: Phys. Lett. B **332**, 20 (1994)
110. R. Schneider et al.: 'Identification and Decay Measurements of ^{100}Sn and Neighbouring Nuclei'. In: *Proc. Intern. Conf. on Exotic Nuclei and Atomic Masses (ENAM 95), June 19–23, 1995*, ed. by M. de Saint Simon, O. Sorlin (Editions Frontières, Gif–sur–Yvette 1995) pp. 565–570
111. M. Chartier et al.: Z. Phys. A **342**, 43 (1992)
112. D. Rudolph et al.: Eur. Phys. J. A **15**, 161 (2002)
113. D. Rudolph et al.: Phys. Rev. C **56**, 98 (1997)
114. C. Chandler et al.: Phys. Rev. C **56**, 2924(R) (1997)
115. F. Becker et al.: Eur. Phys. J. A **4**, 103 (1999)
116. E. Bouchez et al.: Phys. Rev. Lett. **90**, 082502 (2003)
117. Yu.N. Novikov et al.: Eur. Phys. J. A **11**, 257 (2001)
118. K. Schmidt et al.: Z. Phys. A **350**, 99 (1994)
119. M. La Commara et al.: Nucl. Phys. A **708**, 67 (2002)
120. C. Plettner et al.: Nucl. Phys. A **733**, 20 (2004)